The EUMETSAT Network of Satellite Application Facilities

GRAS SAF
GRAS Meteorology

EUMETSAT Satellite Application Facility on GRAS Meteorology

CDOP Visiting Scientist Report 14:
Development of bending angle climatology from RO data

Ulrich Foelsche, Barbara Scherllin-Pirscher

Danish Meteorological Institute (DMI)
European Centre for Medium-Range Weather Forecasts (ECMWF)
Institut d'Estudis Espacials de Catalunya (IEEC)
Met Office (MetO)

Ref: SAF/GRAS/DMI/REP/VS14/001
Version: 1.0
Date: 27 July 2012

DOCUMENT AUTHOR TABLE

	Author(s)	*Function*	*Date*	*Comment*
Prepared by:	Ulrich Foelsche, Barbara Scherllin-Pirscher	GRAS SAF Visiting Scientist	17/07/2012	
Reviewed by:	Stig Syndergaard	GRAS SAF Scientist	27/07/2012	
Approved by:	Kent B. Lauritsen	GRAS SAF Project Manager	27/07/2012	

DOCUMENTATION CHANGE RECORD

Issue / Revision	*Date*	*By*	*Description*
Draft 1	15/03/2012		First draft
Draft 2	15/06/2012		Updated draft
1.0	27/07/2012		Final report

VS Authors
This VS study was carried out by Dr. Ulrich Foelsche, Wegener Center for Climate and Global Change, University of Graz (WEGC/UniGraz), Brandhofgasse 25, A-8010 Graz, Austria, and Institute for Geophysics, Astrophysics, and Meteorology (IGAM)/Institute of Physics, UniGraz; Email: ulrich.foelsche@uni-graz.at and Dr. Barbara Scherllin-Pirscher, also at WEGC and IGAM; Email: barbara.pirscher@uni-graz.at

VS Duration
The VS study was performed during October 2011 to March 2012 and included a one week visit in November 2011 to the Danish Meteorological Institute, Copenhagen, Denmark.

List of Contents

Executive Summary

Current Radio Occultation (RO) retrieval schemes use different types of background data for high altitude initialization, which is unavoidable, if RO data beyond bending angle level are desired. These background data range from exponential extrapolation of the bending angle profile via climatologies to NWP (Numerical Weather Prediction) short-term forecast data. Each approach has advantages but also shortcomings, leading to considerable differences between higher-level RO data from different processing centers. Large biases in the employed high-altitude (above ~30 km) background data lead to notable biases in RO data also at lower altitudes (below ~30 km), due to the downward propagation of errors when performing the Abel integral and the hydrostatic integral. Unbiased high-altitude data, which can be used as a reliable background during the retrieval would therefore be very valuable in order to extend the vertical domain, where derived RO data can still be safely used.

We tested a new approach, based on the assumption that RO data themselves could be used for this purpose, since RO data at altitudes above ~50 km altitude, which are generally too noisy to be used as individual profiles, are still valuable (and largely unbiased), as long as averages over many RO profiles are considered. We found that data from F3C (COSMIC) have sufficient quality for this purpose. The data employed – from August 2006 until July 2011 – have been furthermore gathered in years with low solar activity. The risk of possible contamination due to un-corrected ionospheric errors is therefore low.

We had to perform a reprocessing to obtain the required raw bending angle data, applied a simple, twofold outlier rejection scheme, and tested different ways to combine the new bending angle climatology with additional background information, which is still needed at (even) higher altitudes. Statistical optimization delivers mean bending angle profiles (BAROCLIM), which are reasonably smooth, and make optimal use of the (still) high RO data quality at altitudes between ~50 km and up to ~75 km (where individual profiles are usually not used anymore). Above 80 km BAROCLIM profiles are identical to MSIS climatology profiles, which have been found best-fitting after library search and application of a fitting factor. BAROCLIM is available in NetCDF format, as monthly mean bending angle profiles per 10° latitude bands. We are confident that BAROCLIM will be at least of similar usefulness as the climatologies that are currently used for high-altitude bending angle initialization.

1. Introduction

1.1 Purpose of Document

This document contains the results from a GRAS SAF Visiting Scientist activity from October 2011 to March 2012, with the objective to develop a bending angle climatology from Radio Occultation (RO) data, which can be used for high-altitude initialization within the process of RO profile retrieval.

The document is organized as follows: The remainder of Chapter 1 provides background, context, motivation for the work, and a listing of potential challenges. Chapter 2 describes the development of the bending angle climatology, which is presented in Chapter 3, and validated with analyses from the European Centre for Medium-range Weather Forecasts (ECMWF).

1.2 Background and Context

The value of Radio Occultation (RO) data (*Kursinski et al*., 1997) for climate monitoring is increasingly recognized by the scientific community, since data from different satellites show an amazing degree of consistency, particularly when exactly the same processing scheme is applied (e.g., *Foelsche et al*., 2011). RO data from different centers, however, show slightly larger differences, which are caused by different retrieval schemes (structural uncertainty). One of the most important reasons for such differences are different approaches for high-altitude initialization (*Ho et al*., 2009; 2012; *Steiner et al*., 2012).
The retrieval step from bending angle to refractivity requires background information, since the underlying Abel transform (*Fjeldbo et al*., 1971) relies on bending angle data up to infinity. Actual data certainly do not extend so far, and in practice they are of little use above a certain (mission-dependent) altitude, where individual profiles start being too noisy. Current retrieval schemes use different types of background data, from exponential extrapolation of the bending angle profile via climatologies to NWP (Numerical Weather Prediction) short-term forecast data (see *Ho et al*., 2012 ; *Steiner et al*., 2012;). Each approach has advantages but also shortcomings: Exponential extrapolation requires no external background information but corresponds to the (incorrect) assumption of an isothermal atmosphere. The use of a static climatology, e.g., leads to a time-varying bias at high altitudes, as the stratosphere cools due to climate change (*Foelsche et al*., 2008). Climatological mean profiles will furthermore not provide a good fit in situations like Sudden Stratospheric Warmings (SSW). Background profiles based on NWP forecasts can deal with the latter, but could introduce high-altitude biases in a climate record, when the forecast scheme is changed.
When high-altitude initialization of the Abel integral is done via statistical optimization (*Rieder and Kirchengast*, 2001; *Healy*, 2001), the observations are inversely weighted with the measurement error. As a consequence, the transition height between the measurement dominated and the background dominated regime increases, when the data quality is good. For data from the GRAS instrument (GNSS Receiver for Atmospheric Sounding) onboard Metop (Meteorological Operational satellite) it can be as high as 70 km (*Pirscher*, 2010).
Any bias in the background profile will result in a bias in the retrieved profile down to an altitude that depends on the noise of the data. In this case, we have to expect systematic differences between RO data from receivers with different noise characteristics at altitudes above ~30 km – even if the RO data themselves are unbiased (*Foelsche et al*., 2009).

Therefore it would be very valuable to have unbiased data at high altitudes, which can be used as background for the high-altitude initialization of RO data. This would minimize inter-satellite differences (when the receivers have different noise characteristics) as well as inter-center differences.
One possible strategy to get such a climatology – which has also been pursued in this work – is based on the assumption, that RO data at altitudes above ~50 km altitude, which are generally too noisy to be used as individual profiles, are still valuable (and largely unbiased), as long as averages over many RO profiles are considered. Related ideas have been discussed for quite a while in the scientific RO community and we are e.g. aware of early discussions with scientists from the COSMIC group at UCAR (University Corporation for Atmospheric Research, Boulder, Colorado, USA) and with Michael Gorbunov (Obukhov Institute for Atmospheric Physics, Moscow, Russia). *Ao et al*. (2012) and *Gleisner and Healy* (2012) have proposed an alternative approach for obtaining RO climatologies, where RO profiles are already averaged at bending angle level, and the Abel transform is then applied to this mean bending angle profile in order to obtain a mean refractivity profile. COSMIC data have sufficiently small noise, so that the average profile is reasonably smooth and can be converted to refractivity without performing statistical optimization. This approach can, however, not be applied to CHAMP data, which have a significantly higher noise level (see also section 2.1 below). At the present date climate monitoring based on RO data is futile without incorporating the CHAMP data record – we therefore followed a different approach, where the high-quality COSMIC data are used to build a representative mean bending angle climatology – which can then also be used as high-altitude background for the inversion of CHAMP RO data.

1.3 Motivation and Challenges

This section is repeated (and just slightly adapted for consistency) from the GRAS SAF CDOP Visiting Scientist Proposal No. 14 by Kent B. Lauritsen and Stig Syndergaard (in *italic*). It describes the motivation for the work and several potential challenges, foreseen by the proposers. Throughout the report we will also describe how we dealt with the indicated challenges.

1.3.1 Motivation

Statistical optimization (SO) is necessary to obtain accurate and unbiased refractivity profiles in the stratosphere and above because the processing step from bending angle to refractivity includes formally an integration of the bending angle to infinitely high altitudes. This is normally accomplished by extending the observed bending angle profile to very high altitudes using a bending angle climatological model.
The SO ensures a smooth transition between the model profile and the observed profile based on assumed or estimated error co-variances of the model and the observations. However, if the model profile is biased significantly it can introduce a fractional bias in retrieved refractivity down through the stratosphere. To avoid such added refractivity biases, it is important, for each occultation, to use a model profile that resembles the large-scale variations in the data (assuming that the data on average are correct, but contaminated with small-scale random noise) up to at least 60 km. It is beneficial if the model profile resembles accurately the true neutral atmospheric bending angle above this altitude.

For the SO, the GRAS SAF uses a spectral representation of the MSIS90 climatological model transformed to bending angle space. The model profile used in the SO for a given occultation is found through a global search in the MSIS bending angle model. In this process the MSIS bending angles are scaled and shifted (in bending angle log-space) in a least squares fit to the observed (non-optimized) LC bending angle between 40 and 60 km.

There is today a very large amount of RO data from missions like CHAMP, COSMIC and Metop. Of those, CHAMP and COSMIC measurements generally go to altitudes of about 120 km, whereas Metop measurements only exist up to about 80 km. Already several years ago UCAR scientists started speculating if this large amount of RO data (at the time only for CHAMP) could be used to generate an improved climatological bending angle model that can be used for SO in the retrieval of refractivity.

1.3.2 Potential Challenges

1) There is some uncertainty concerning the feasibility of deriving a fully bias-free climatology based entirely on RO data. Nevertheless, a climatology derived from raw RO bending angles should be at least of similar usefulness as the climatologies that are currently used.

2) It is not clear to what extent residual ionospheric systematic errors might pose a problem. Neutral atmospheric bending angles are derived via ionospheric correction of L1 and L2 bending angles. Even so, sensitivity in LC bending angles to day-night variations at altitudes between 60 and 80 km has been reported by scientists at UCAR, presumable because of ionospheric diurnal variability. Similarly, it is expected that the LC bending angles are contaminated with a systematic residual error following the 11-year solar cycle.

3) The model at high altitudes would have to be very smooth and without unphysical wiggles. Since the bending angle decreases basically exponentially with altitude, random noise becomes an increasing problem with altitude. Thus, a very large amount of RO data must be averaged and smoothed, and although there is a vast amount of RO data available, the distribution in time and space reduces the available profiles for a given location and time and thus the precision that can be obtained might be limited. At some high altitude it will be necessary to merge the data with some already existing model to fulfill the requirement that the model be smooth and accurate to high altitudes, also in a fractional sense.

4) Large outliers (e.g., because of strong ionospheric scintillations that might still be present to some extent in the raw bending angle LC data) would have to be detected and eliminated from the analysis.

5) A full reprocessing of available (used in this study) RO data may be necessary, since the existing databases of bending angles for CHAMP, COSMIC and other missions at UCAR contains bending angles only up to 60 km. This would not be sufficient to study e.g., the solar cycle signature.

6) Validation of the model might be a challenge since it is not clear what one would compare against. One option would be the NCAR climatology; another would be to verify if bias and standard deviation against ECMWF is reduced when using the new model in the SO in retrieval of refractivity.

2. Development of a Bending Angle Climatology

2.1 Feasibility

In a first step, we checked the principal feasibility of the proposed approach (see challenge 1 in section 1.3.2) by computing raw bending angle climatologies with the WEGC CLIPS software (Climatology Processing System, see *Pirscher*, 2010). Since there are no raw bending angle data beyond 60 km altitude available (as foreseen in challenge 5), we had to perform a reprocessing of our RO data to obtain bending angle profiles up to 120 km altitude. The reprocessing was first performed for individual months (July 2007 to 2010), and terminated after bending angle calculation, to ensure timeliness of the results.

Operationally, we provide optimized bending angles (via *www.globclim.org*). The software was therefore adapted to compute zonal mean climatologies of raw bending angels as well. Figure 1 shows examples for the test month July 2007 with 10° latitudinal resolution, up to an impact altitude of 120 km. The overall behavior shows, that data from the CHAMP satellite (CHAllenging Minisatellite Payload for geoscientific research) above ~60 km are certainly too noisy to provide the desired high-altitude data (left). Data from the FORMOSAT-3/ COSMIC constellation (Formosa Satellite Mission 3/Constellation Observing System for Meteorology, Ionosphere and Climate, F3C hereinafter), on the other hand (right), seem to provide meaningful information up to at least 70 km altitude. Based on these initial results we decided to proceed, but to discard CHAMP data from the further analysis. The resulting bending angle climatology is therefore entirely based on F3C bending angle data. F3C data have been available from August 2006 until July 2011 – corresponding to years with low solar activity. The risk of possible contamination due to un-corrected ionospheric errors is therefore low (see challenge 2).

Further evidence for this assumption comes from initial results on residual systematic ionospheric errors in RO data (*Schreiner et al.*, 2011; *Danzer et al.*, 2012). Danzer et al. (2012) looked at bending angles from early 2002 until mid-2011 between 65 km and 80 km (impact) altitude. In this altitude range, the bending due to the neutral atmosphere is already small, and systematic differences can be largely explained by un-corrected ionospheric errors.

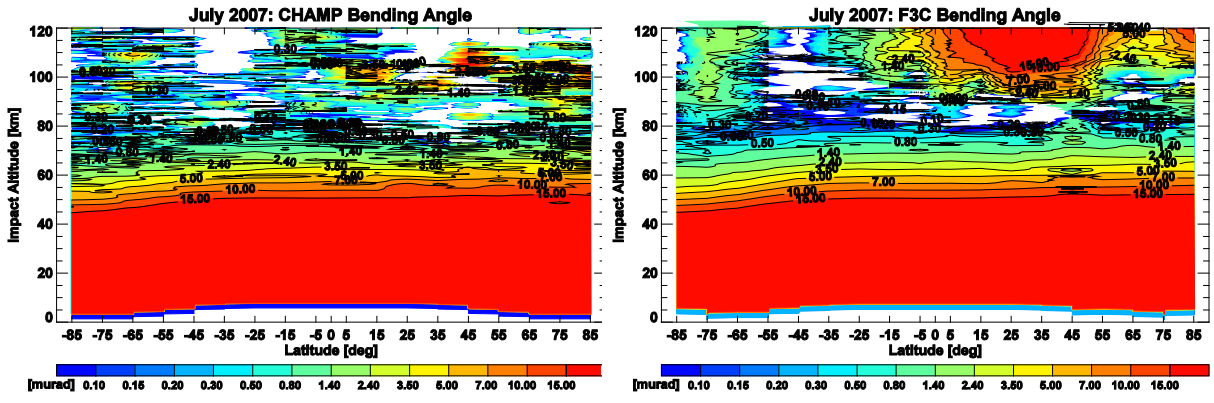

Fig. 1. Raw bending angle climatology for July 2007 based on CHAMP (left) and F3C (right) RO profiles.

Daytime bending angle values show a clear dependence on the solar cycle, while nighttime values remain surprisingly stable over the entire time period from high (early 2002) to very low solar activity (2006 to 2010). The difference between daytime and nighttime bending angles, which can therefore be regarded as a good indicator for uncorrected systematic ionospheric errors, reaches up to –0.4 µrad during high solar activity, but generally remains below –0.1 µrad during the time period used for the present study.

For the raw bending angle climatologies shown in Fig. 1, we used all existing profiles, which could be successfully computed. A closer inspection of the results for F3C showed however, that comparatively few outliers (which, however, "survived" the bending angle retrieval) can lead to un-physical results, like the "red" region above 100 km at low to mid northern latitudes in the right panel of Fig. 1. Furthermore, "white" patches above ~80 km correspond to negative bending angles – which clearly shows that additional background information is needed at higher altitudes.

2.2 Outlier Rejection

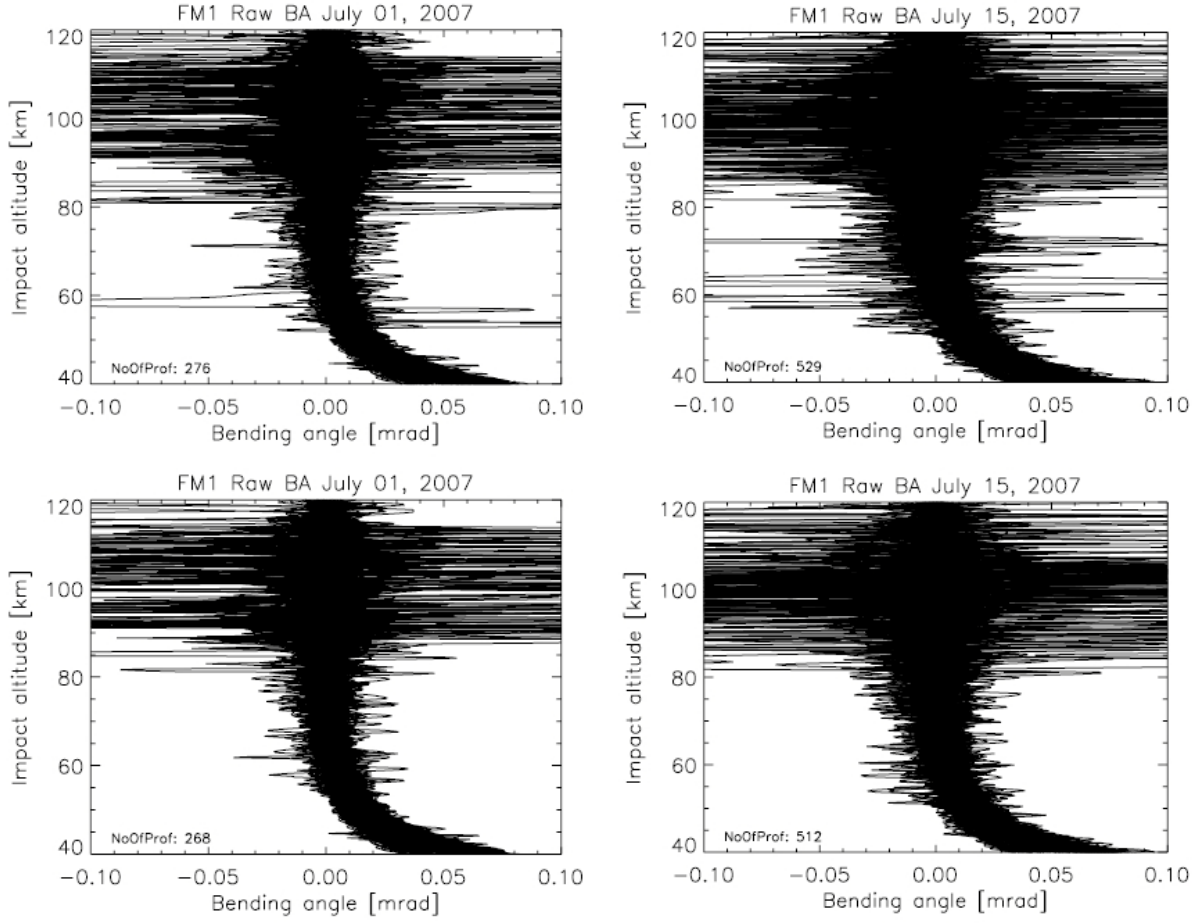

Fig. 2. Raw bending angles from the F3C satellite FM-1 for July 1, 2007 (left) and July 15, 2007 (right): All profiles (top) and after rejection of those profiles, which did not meet the 40 µrad in the altitude range 50 km to 80 km (bottom).

Based on the results shown in section 2.1 (see also challenge 4) we introduced a twofold approach for outlier rejection (in the operational WEGC retrieval the un-physical RO profiles would have been rejected in later steps of the retrieval chain).

In a first step we rejected all profiles with bending angles larger than 40 µrad or smaller than –40 µrad in the altitude range 50 km to 80 km. Figure 2 shows, as examples, globally distributed profiles from the F3C satellite FM-1 (Flight Model-1) on two days in the test month July 2007 before (top) and after (bottom) application of the 40 µrad criterion. While only 8 of 276 profiles (July 1) and 17 of 529 profiles (July 15) are affected, the obvious outliers are clearly removed. After several tests we decided to apply the 40 µrad criterion up to an altitude of 90 km for the final realization (see Fig. 3).

In a second step, we rejected all profiles that showed bending angles outside of 4 standard deviations from the mean in the entire altitude range. We additionally tested the performance for the July months 2008, 2009, and 2010, as exemplarily illustrated in Fig. 3: The top panel shows all F3C profiles in July 2008, in the latitude bin 10°S to 20°S, after application of the 40 µrad criterion (thick red line: median of all profiles, thick green line: mean, thick yellow line: one standard deviation, thin yellow line: 4 standard deviations). The bottom panel shows the effect of the 4σ rejection (affecting 776 of 3555 profiles, ~22 %), which resulted in a considerable decrease in standard deviation, especially above 90 km altitude (since the 40 µrad criterion in step 1 has only been applied up to an impact altitude of 90 km).

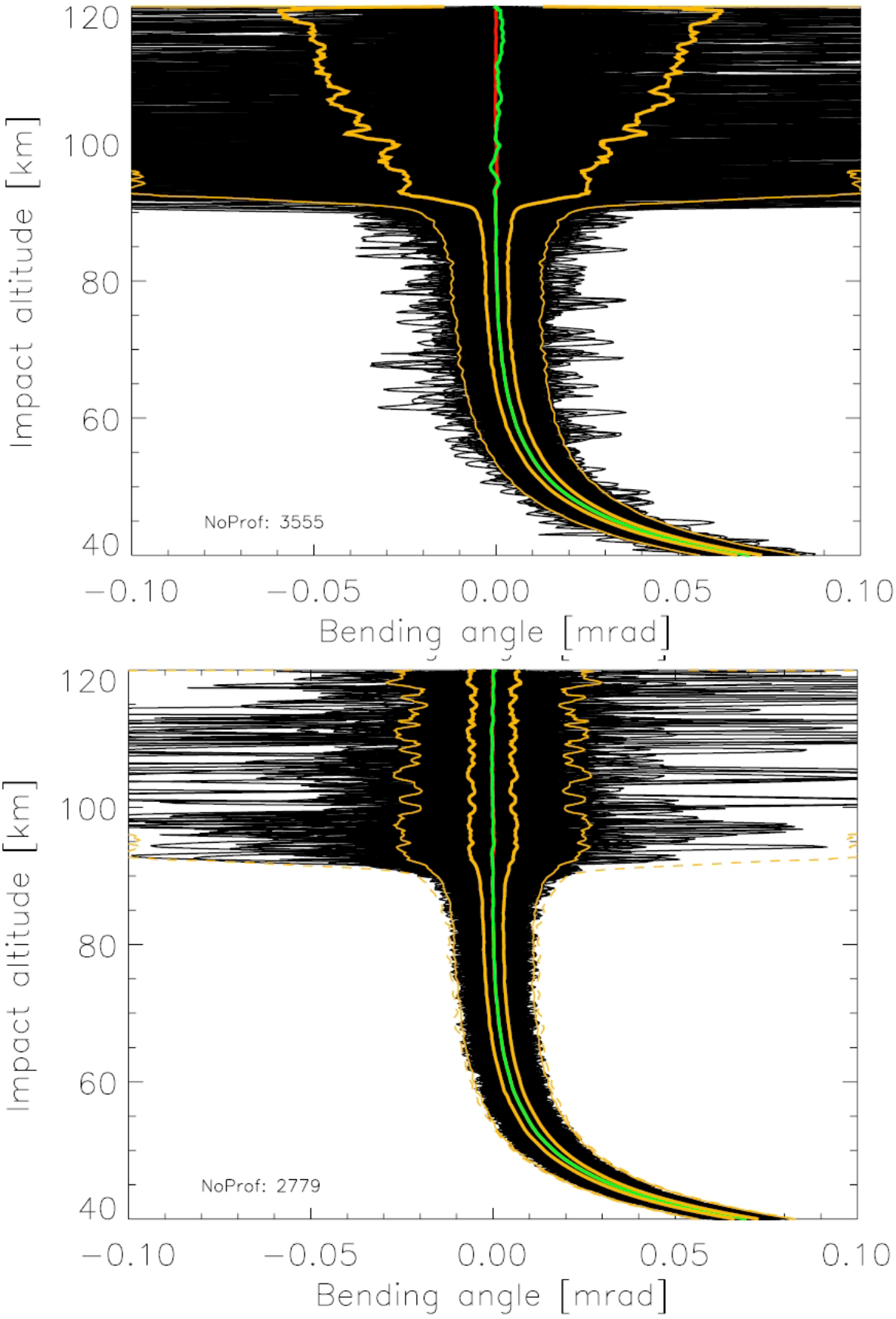

Fig. 3. F3C RO bending angle profiles in July 2008 in the latitude bin 10°S to 20°S before (top) and after the application of the 4σ outlier rejection criterion (bottom). See text for further explanation.

2.3 Raw Bending Angle Climatology

Bending angle profiles within 18 latitude bins (10° width, from pole to pole) have then be used (after outlier rejection – see section 2.2) to compute mean profiles for the individual test months (July 2007 to 2010). Figure 4 illustrates, that using a mean (red) of these four individual monthly mean profiles (green) reduces the vertical variability. But even this mean profile is not yet smooth enough to be used as background profile above ~70 km altitude (see challenge 3). Furthermore, (unphysical) negative bending angles appear above ~82 km altitude.

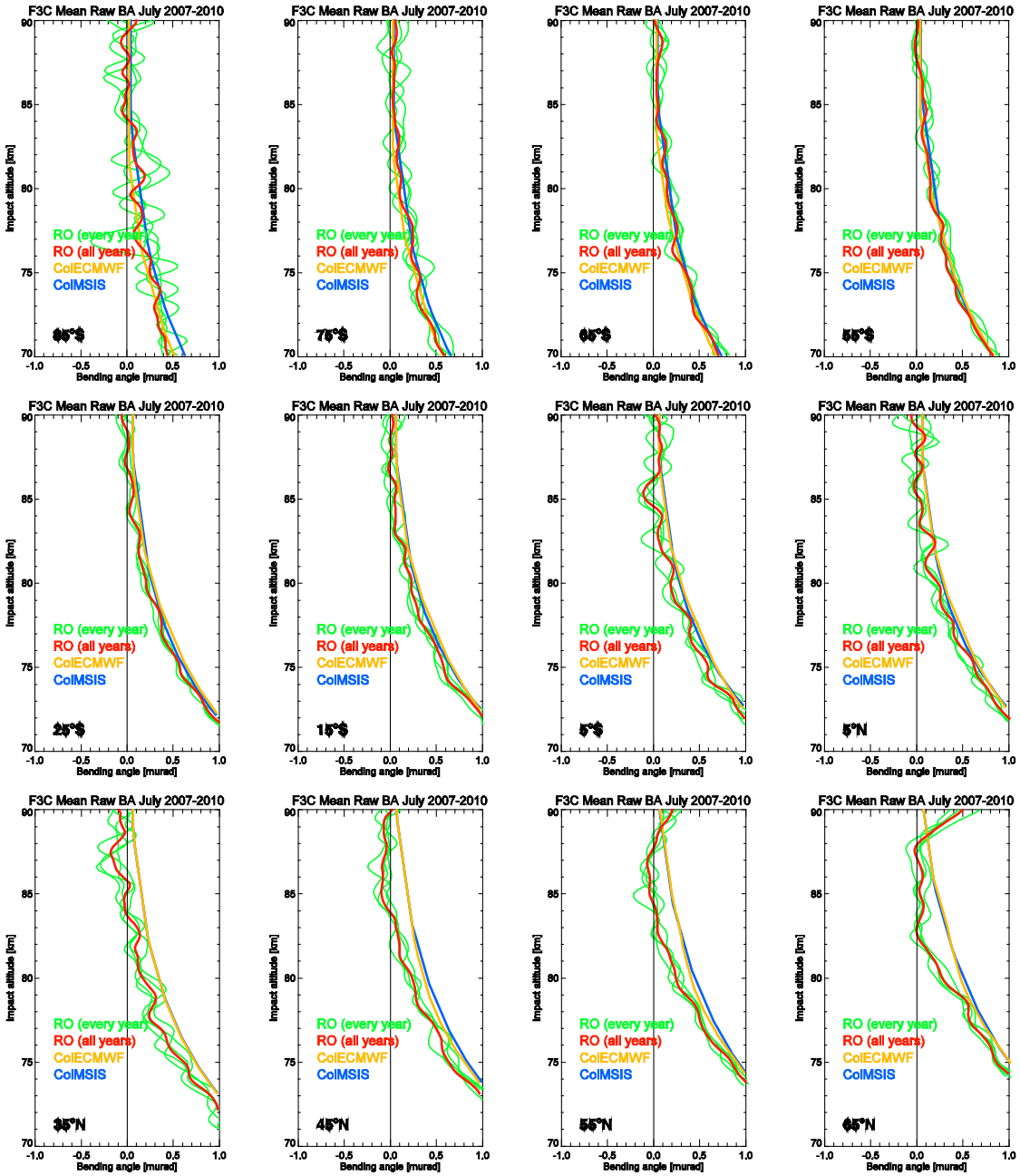

Fig. 4. Monthly mean RO bending angle profiles for July 2007 to 2010 (green), mean profile over these 4 months (red), co-located mean MSIS profile (blue), and co-located mean ECMWF profile (yellow).

2.4 Additional High-Altitude Information

Because of (unphysical) negative bending angles above ~82 km (section 2.3) the raw bending angle climatology has to be combined with additional data, like the MSIS-90 climatology (*Hedin*, 1991) at high altitudes. ECMWF analysis profiles in L91 vertical resolution extend only up to ~80 km altitude, and also need to be combined with additional high-altitude information (like – again – MSIS, as shown here). We therefore decided to use MSIS climatology throughout.

In order to make maximum use of the information content of the RO data – where their quality is superior to the MSIS climatology information – we do not use co-located MSIS profiles, but perform a library search to find the best-fitting MSIS profile (in the altitude range, where RO data quality is still high), which is additionally multiplied with a fit factor. Figure 5 shows an illustrative example with a small fit-factor (in this case the search algorithm could only choose among July mean profiles in the different latitude bins. In the final realization fit factors are closer to 1, since the search algorithm can find better fitting MSIS profiles also in other months).

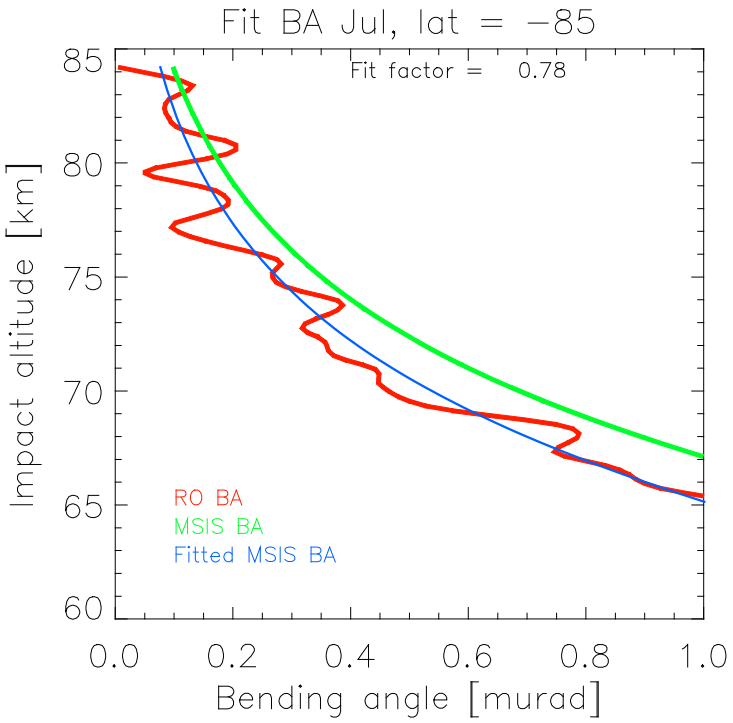

Fig. 5. July-mean RO bending angle profile (red), library-searched MSIS profile (green), and search-fitted MSIS profile (green) in the southernmost latitude bin (80°S to 90°S).

2.5 Combining Bending Angles with the Additional Background

We tried different approaches to combine bending angle data and background climatology in an optimal way, e.g., by using a Gaussian transition. Figure 6 shows the results for the same (difficult) bin as in Fig. 5. The transition is performed in the altitude interval between 65 km and the level where the first negative bending angles appear immediately above (84 km in this case). The weighting function is shown in the right panel, where the Gaussian half width is (maxOptLevel – minOptLevel)/2.5. This approach clearly fails to remove the wiggles from the resulting profile.

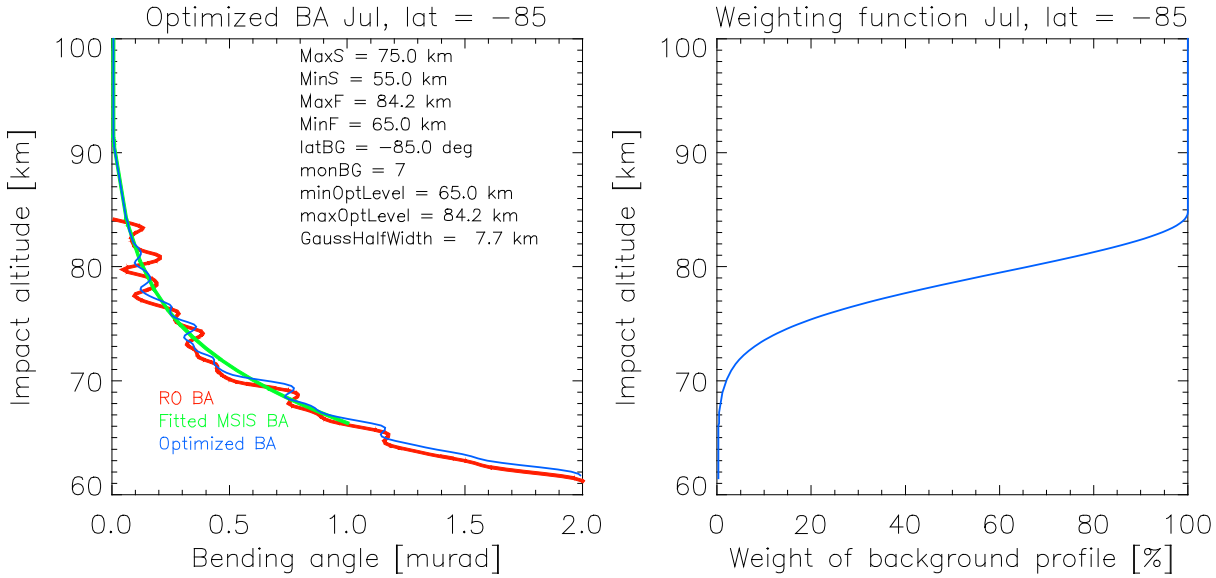

Fig. 6. Gaussian transition between RO bending angles and MSIS climatology.

We obtained the best results performing statistical optimization by inverse covariance weighting. Figure 7 shows the result for the same bin as in Fig. 6, already in the final setup, where we could use all reprocessed data – five full years of F3C bending angle data from August 2006 until July 2011. Search and fit (see section 2.4) was performed between 60 km and 80 km altitude, in this case the best-fitting profile was found in June.

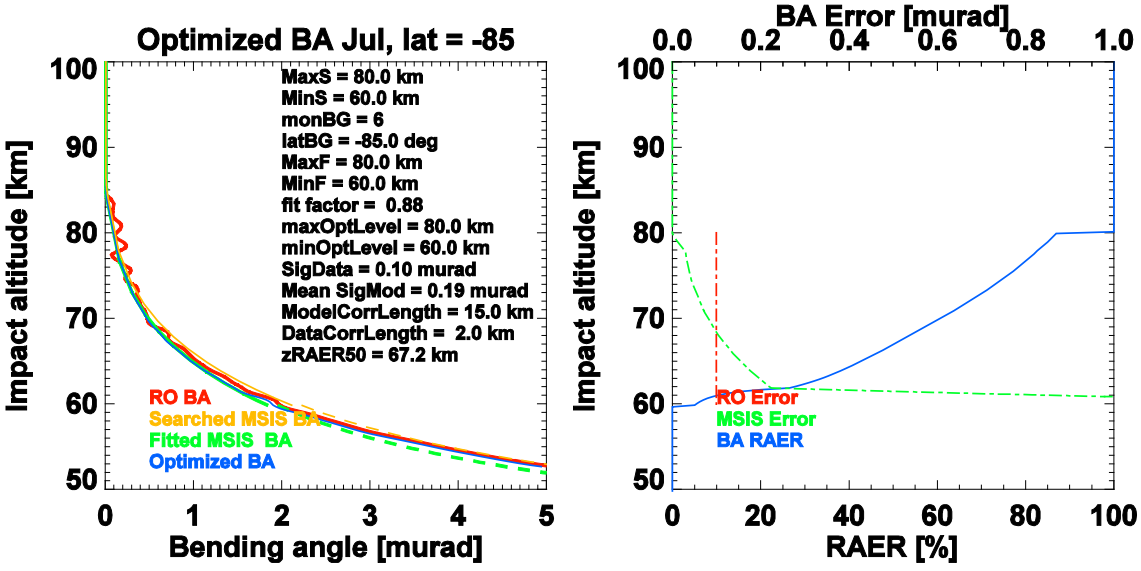

Fig. 7. Statistical optimization of RO bending angles and MSIS background for July (80°S to 90°S).

We used a data correlation length (L_{obs}) of 2 km and a model correlation length (L_{bg}) of 15 km. The background error (σ_{bg}, green line in the right panel of Fig. 7, referring to the upper x-axis) increases linearly from 0 % at 80 km to 15 % at 78 km (to avoid a too sharp transition), and then again from 15 % at 62 km to 100 % at 60 km (% values refer to the absolute value of the background bending angle profile at the respective altitude level). The observational error (σ_{obs}, red line in the right panel of Fig. 7) was estimated to be the mean background error between 62 km and 78 km impact altitude – applied constant with height, which assures data-domination at lower, and background-domination at higher altitudes. The blue line in the right panel is **not** a weighting function (like in the right panel of Fig. 6), but the "Retrieval to Apriori Error Ratio" (*RAER*), a measure of relative importance of background and observation:

$$RAER = 100\frac{\sigma_{ret}}{\sigma_{bg}}\ , \qquad (1)$$

where σ_{ret} contains the square root of the diagonal elements of the retrieval error covariance matrix **R**, which is given by

$$\mathbf{R} = \left(\mathbf{B}^{-1} + \mathbf{O}^{-1}\right)^{-1}, \qquad (2)$$

where the background error covariance matrix (**B**) and the observation error covariance matrix (**O**) are given by:

$$\mathbf{B}_{ij} = \sigma_{bg(i)}\sigma_{bg(j)}\ \exp\left(-\frac{\left|a_i + a_j\right|}{L_{bg}}\right)$$
$$\mathbf{O}_{ij} = \sigma_{obs(i)}\sigma_{obs(j)}\ \exp\left(-\frac{\left|a_i + a_j\right|}{L_{obs}}\right), \qquad (3)$$

a being the impact parameter at levels *i* and *j*, respectively. zRAER50 is the impact altitude, where retrieval to a priori error ratio equals 50 %, corresponding to the transition from data-domination to background-domination (in this case 67.2 km).

The statistical optimization results for July in the other bins are shown on the next pages (from North to South). Results for January, April and October are furthermore contained in Appendix A.

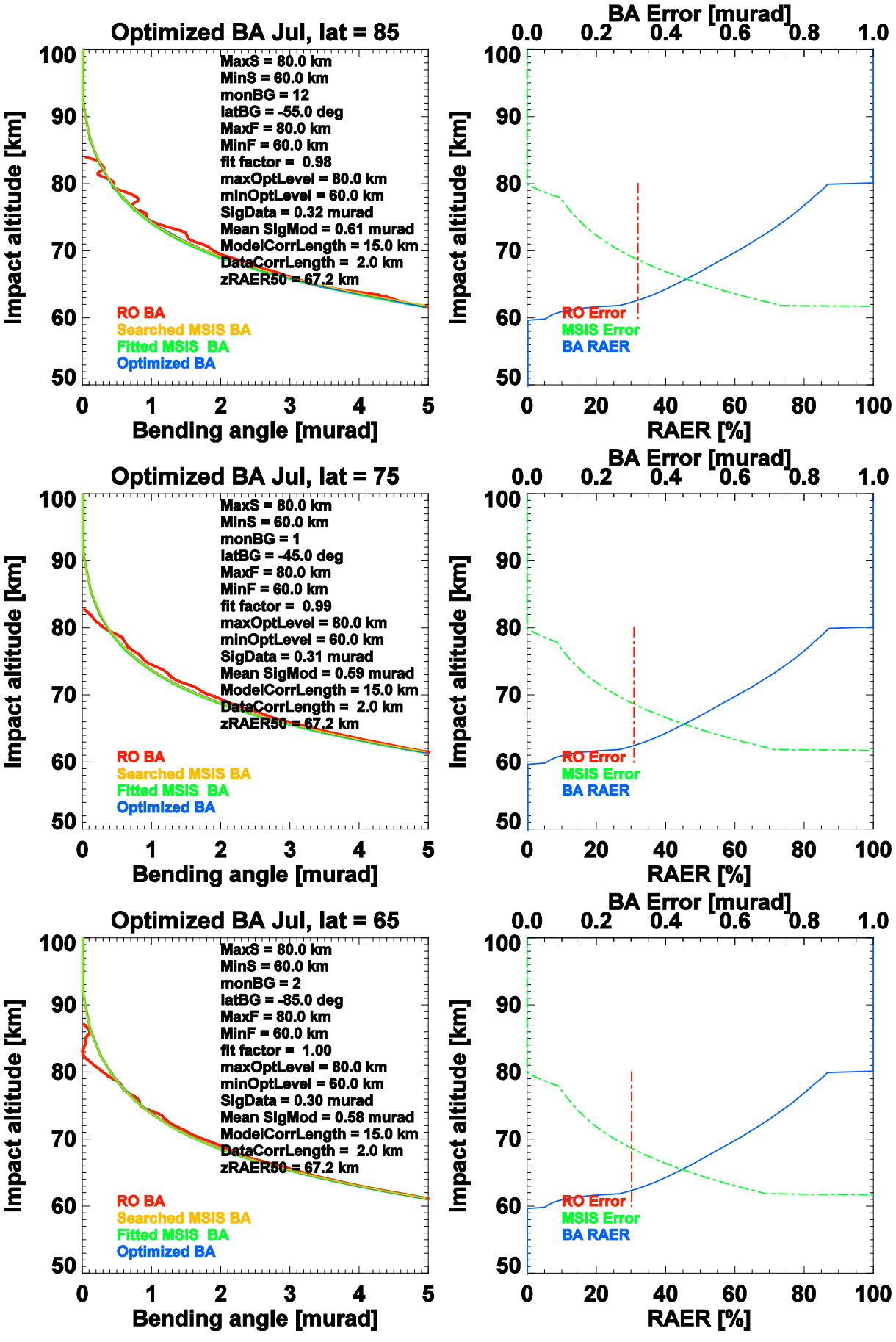
Optimized BA Jul, lat = 85
MaxS = 80.0 km
MinS = 60.0 km
monBG = 12
latBG = -55.0 deg
MaxF = 80.0 km
MinF = 60.0 km
fit factor = 0.98
maxOptLevel = 80.0 km
minOptLevel = 60.0 km
SigData = 0.32 murad
Mean SigMod = 0.61 murad
ModelCorrLength = 15.0 km
DataCorrLength = 2.0 km
zRAER50 = 67.2 km
RO BA
Searched MSIS BA
Fitted MSIS BA
Optimized BA
Impact altitude [km]
Bending angle [murad]
BA Error [murad]
RO Error
MSIS Error
BA RAER
RAER [%]
Optimized BA Jul, lat = 75
MaxS = 80.0 km
MinS = 60.0 km
monBG = 1
latBG = -45.0 deg
MaxF = 80.0 km
MinF = 60.0 km
fit factor = 0.99
maxOptLevel = 80.0 km
minOptLevel = 60.0 km
SigData = 0.31 murad
Mean SigMod = 0.59 murad
ModelCorrLength = 15.0 km
DataCorrLength = 2.0 km
zRAER50 = 67.2 km
Optimized BA Jul, lat = 65
MaxS = 80.0 km
MinS = 60.0 km
monBG = 2
latBG = -65.0 deg
MaxF = 80.0 km
MinF = 60.0 km
fit factor = 1.00
maxOptLevel = 80.0 km
minOptLevel = 60.0 km
SigData = 0.30 murad
Mean SigMod = 0.58 murad
ModelCorrLength = 15.0 km
DataCorrLength = 2.0 km
zRAER50 = 67.2 km

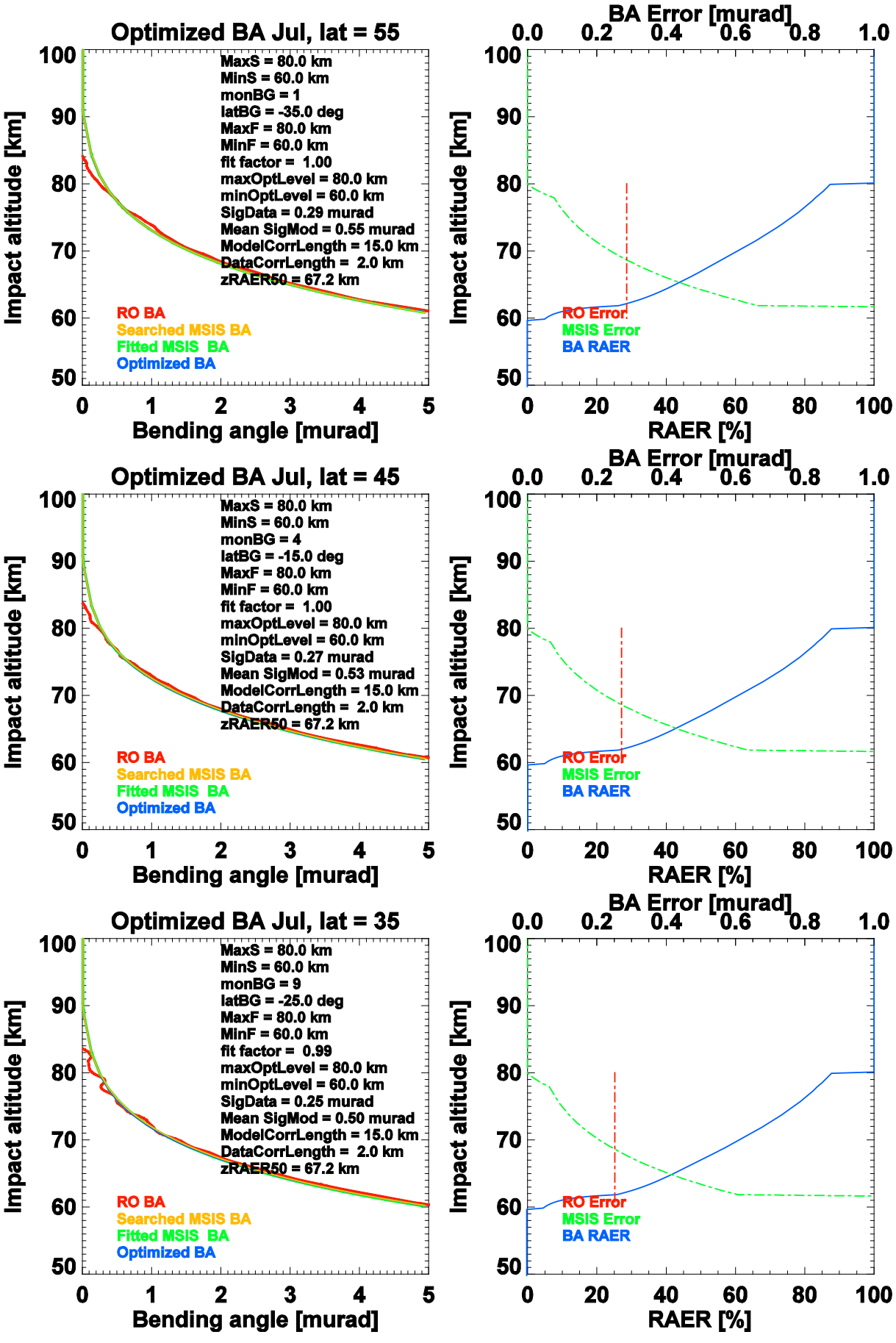
Optimized BA Jul, lat = 55
MaxS = 80.0 km
MinS = 60.0 km
monBG = 1
latBG = -35.0 deg
MaxF = 80.0 km
MinF = 60.0 km
fit factor = 1.00
maxOptLevel = 80.0 km
minOptLevel = 60.0 km
SigData = 0.29 murad
Mean SigMod = 0.55 murad
ModelCorrLength = 15.0 km
DataCorrLength = 2.0 km
zRAER50 = 67.2 km
RO BA
Searched MSIS BA
Fitted MSIS BA
Optimized BA
Impact altitude [km]
Bending angle [murad]
BA Error [murad]
RO Error
MSIS Error
BA RAER
RAER [%]
Optimized BA Jul, lat = 45
MaxS = 80.0 km
MinS = 60.0 km
monBG = 4
latBG = -15.0 deg
MaxF = 80.0 km
MinF = 60.0 km
fit factor = 1.00
maxOptLevel = 80.0 km
minOptLevel = 60.0 km
SigData = 0.27 murad
Mean SigMod = 0.53 murad
ModelCorrLength = 15.0 km
DataCorrLength = 2.0 km
zRAER50 = 67.2 km
Optimized BA Jul, lat = 35
MaxS = 80.0 km
MinS = 60.0 km
monBG = 9
latBG = -25.0 deg
MaxF = 80.0 km
MinF = 60.0 km
fit factor = 0.99
maxOptLevel = 80.0 km
minOptLevel = 60.0 km
SigData = 0.25 murad
Mean SigMod = 0.50 murad
ModelCorrLength = 15.0 km
DataCorrLength = 2.0 km
zRAER50 = 67.2 km

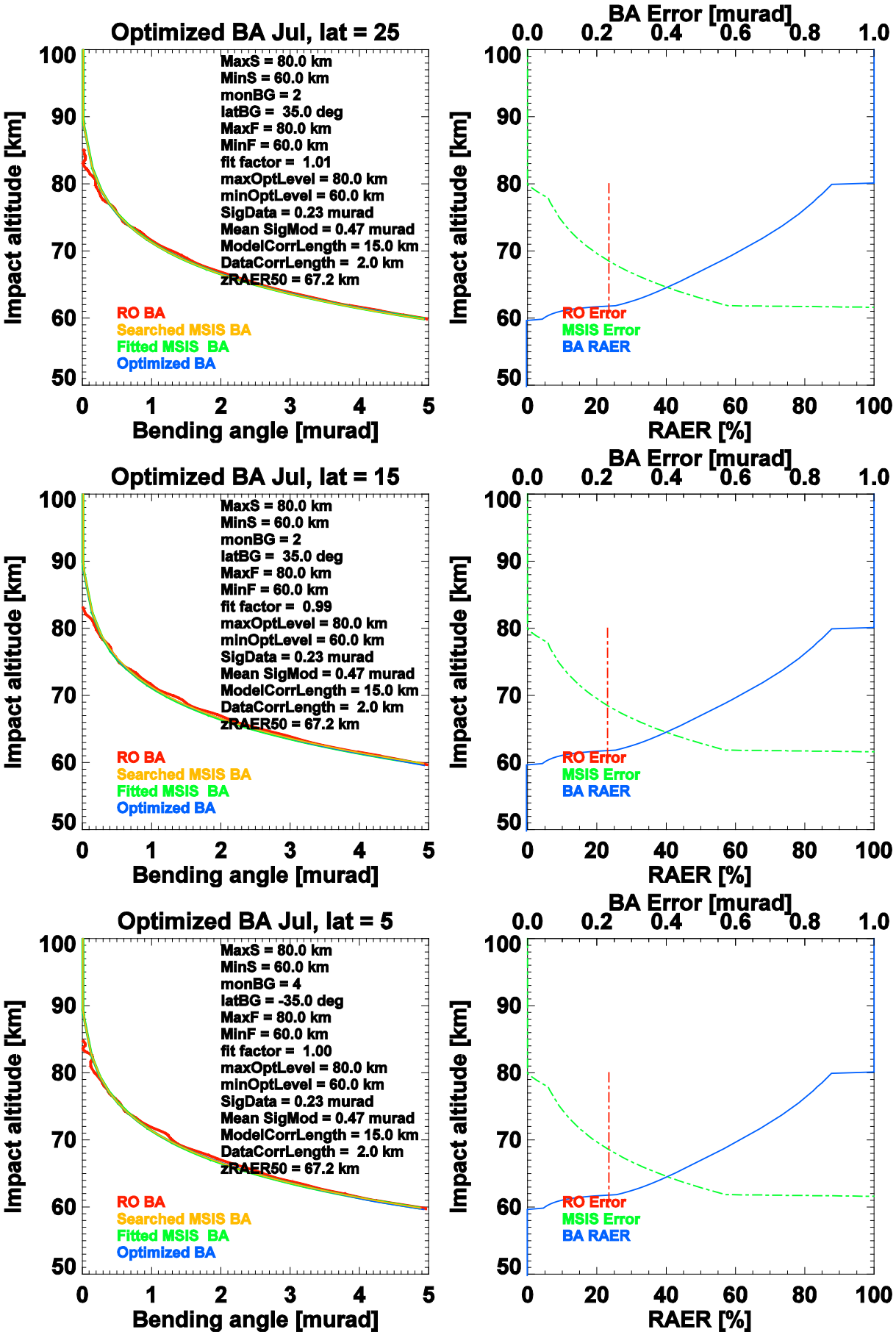
Optimized BA Jul, lat = 25
MaxS = 80.0 km
MinS = 60.0 km
monBG = 2
latBG = 35.0 deg
MaxF = 80.0 km
MinF = 60.0 km
fit factor = 1.01
maxOptLevel = 80.0 km
minOptLevel = 60.0 km
SigData = 0.23 murad
Mean SigMod = 0.47 murad
ModelCorrLength = 15.0 km
DataCorrLength = 2.0 km
zRAER50 = 67.2 km
RO BA
Searched MSIS BA
Fitted MSIS BA
Optimized BA
Impact altitude [km]
Bending angle [murad]
BA Error [murad]
RO Error
MSIS Error
BA RAER
RAER [%]
Optimized BA Jul, lat = 15
MaxS = 80.0 km
MinS = 60.0 km
monBG = 2
latBG = 35.0 deg
MaxF = 80.0 km
MinF = 60.0 km
fit factor = 0.99
maxOptLevel = 80.0 km
minOptLevel = 60.0 km
SigData = 0.23 murad
Mean SigMod = 0.47 murad
ModelCorrLength = 15.0 km
DataCorrLength = 2.0 km
zRAER50 = 67.2 km
RO BA
Searched MSIS BA
Fitted MSIS BA
Optimized BA
Impact altitude [km]
Bending angle [murad]
BA Error [murad]
RO Error
MSIS Error
BA RAER
RAER [%]
Optimized BA Jul, lat = 5
MaxS = 80.0 km
MinS = 60.0 km
monBG = 4
latBG = -35.0 deg
MaxF = 80.0 km
MinF = 60.0 km
fit factor = 1.00
maxOptLevel = 80.0 km
minOptLevel = 60.0 km
SigData = 0.23 murad
Mean SigMod = 0.47 murad
ModelCorrLength = 15.0 km
DataCorrLength = 2.0 km
zRAER50 = 67.2 km
RO BA
Searched MSIS BA
Fitted MSIS BA
Optimized BA
Impact altitude [km]
Bending angle [murad]
BA Error [murad]
RO Error
MSIS Error
BA RAER
RAER [%]

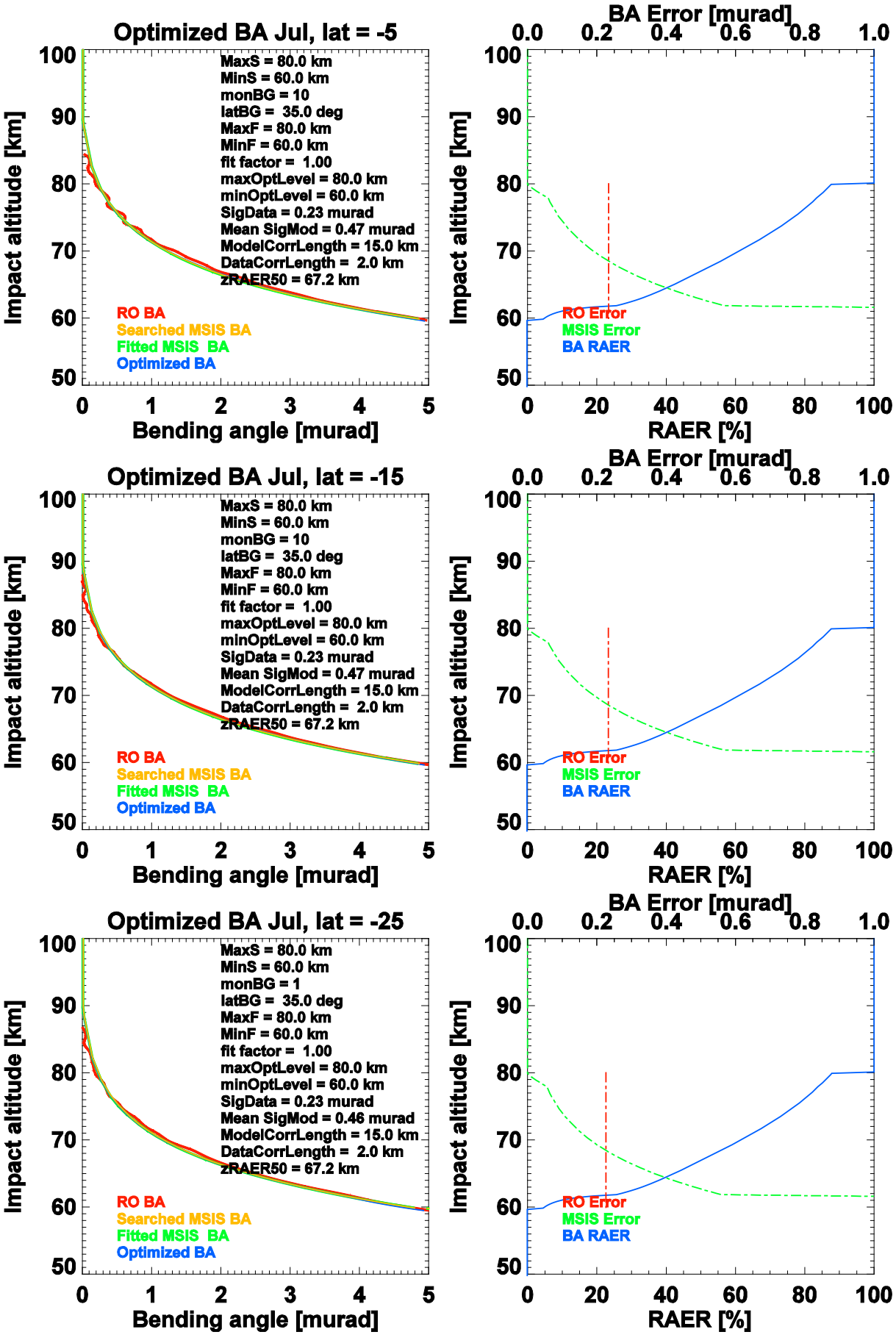
Optimized BA Jul, lat = -5
MaxS = 80.0 km
MinS = 60.0 km
monBG = 10
latBG = 35.0 deg
MaxF = 80.0 km
MinF = 60.0 km
fit factor = 1.00
maxOptLevel = 80.0 km
minOptLevel = 60.0 km
SigData = 0.23 murad
Mean SigMod = 0.47 murad
ModelCorrLength = 15.0 km
DataCorrLength = 2.0 km
zRAER50 = 67.2 km
RO BA
Searched MSIS BA
Fitted MSIS BA
Optimized BA
Impact altitude [km]
Bending angle [murad]
BA Error [murad]
RO Error
MSIS Error
BA RAER
RAER [%]
Optimized BA Jul, lat = -15
Optimized BA Jul, lat = -25
MaxS = 80.0 km
MinS = 60.0 km
monBG = 1
latBG = 35.0 deg
MaxF = 80.0 km
MinF = 60.0 km
fit factor = 1.00
maxOptLevel = 80.0 km
minOptLevel = 60.0 km
SigData = 0.23 murad
Mean SigMod = 0.46 murad
ModelCorrLength = 15.0 km
DataCorrLength = 2.0 km
zRAER50 = 67.2 km

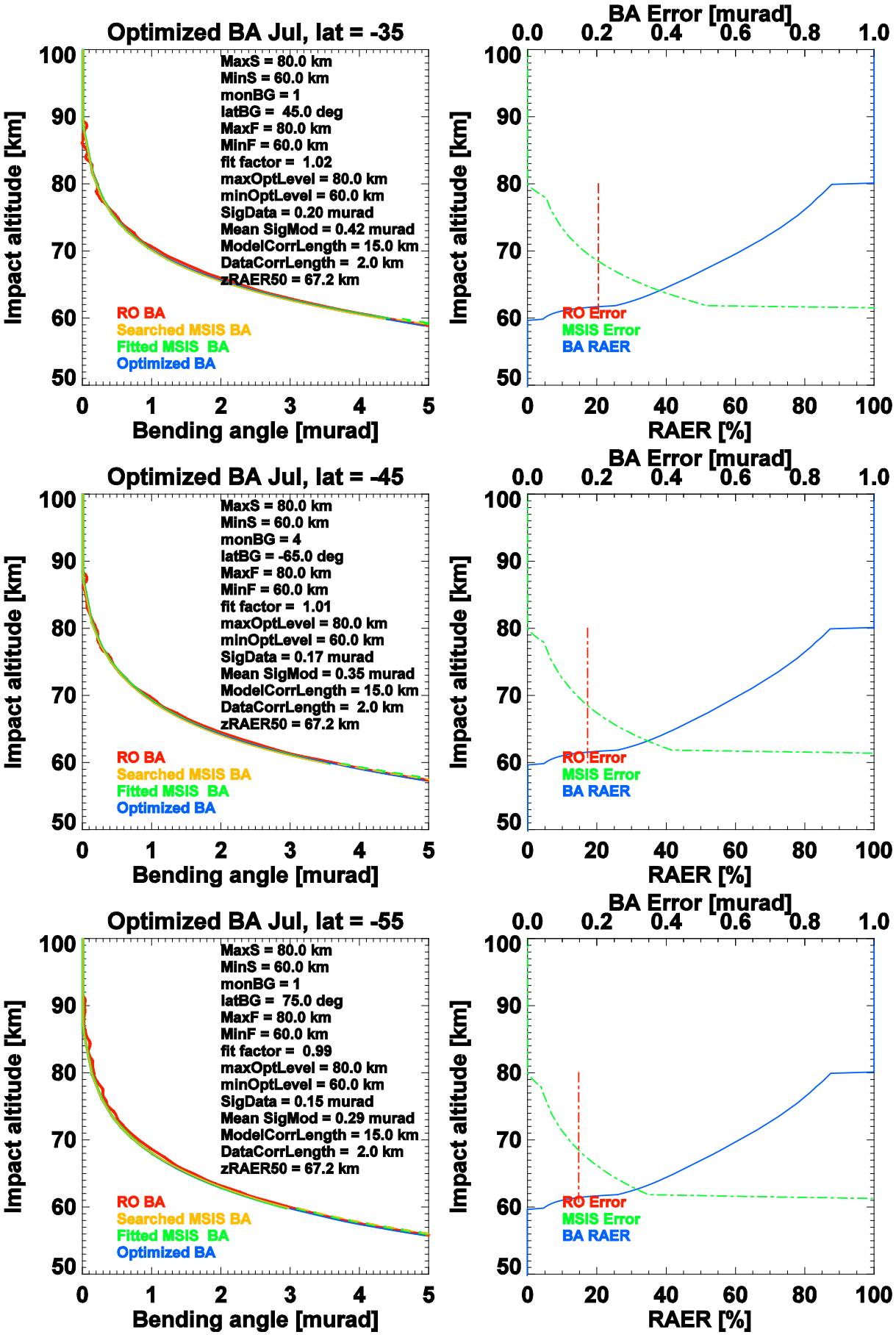
Optimized BA Jul, lat = -35
MaxS = 80.0 km
MinS = 60.0 km
monBG = 1
latBG = 45.0 deg
MaxF = 80.0 km
MinF = 60.0 km
fit factor = 1.02
maxOptLevel = 80.0 km
minOptLevel = 60.0 km
SigData = 0.20 murad
Mean SigMod = 0.42 murad
ModelCorrLength = 15.0 km
DataCorrLength = 2.0 km
zRAER50 = 67.2 km
RO BA
Searched MSIS BA
Fitted MSIS BA
Optimized BA
Impact altitude [km]
Bending angle [murad]
BA Error [murad]
RO Error
MSIS Error
BA RAER
RAER [%]
Optimized BA Jul, lat = -45
MaxS = 80.0 km
MinS = 60.0 km
monBG = 4
latBG = -65.0 deg
MaxF = 80.0 km
MinF = 60.0 km
fit factor = 1.01
maxOptLevel = 80.0 km
minOptLevel = 60.0 km
SigData = 0.17 murad
Mean SigMod = 0.35 murad
ModelCorrLength = 15.0 km
DataCorrLength = 2.0 km
zRAER50 = 67.2 km
Optimized BA Jul, lat = -55
MaxS = 80.0 km
MinS = 60.0 km
monBG = 1
latBG = 75.0 deg
MaxF = 80.0 km
MinF = 60.0 km
fit factor = 0.99
maxOptLevel = 80.0 km
minOptLevel = 60.0 km
SigData = 0.15 murad
Mean SigMod = 0.29 murad
ModelCorrLength = 15.0 km
DataCorrLength = 2.0 km
zRAER50 = 67.2 km

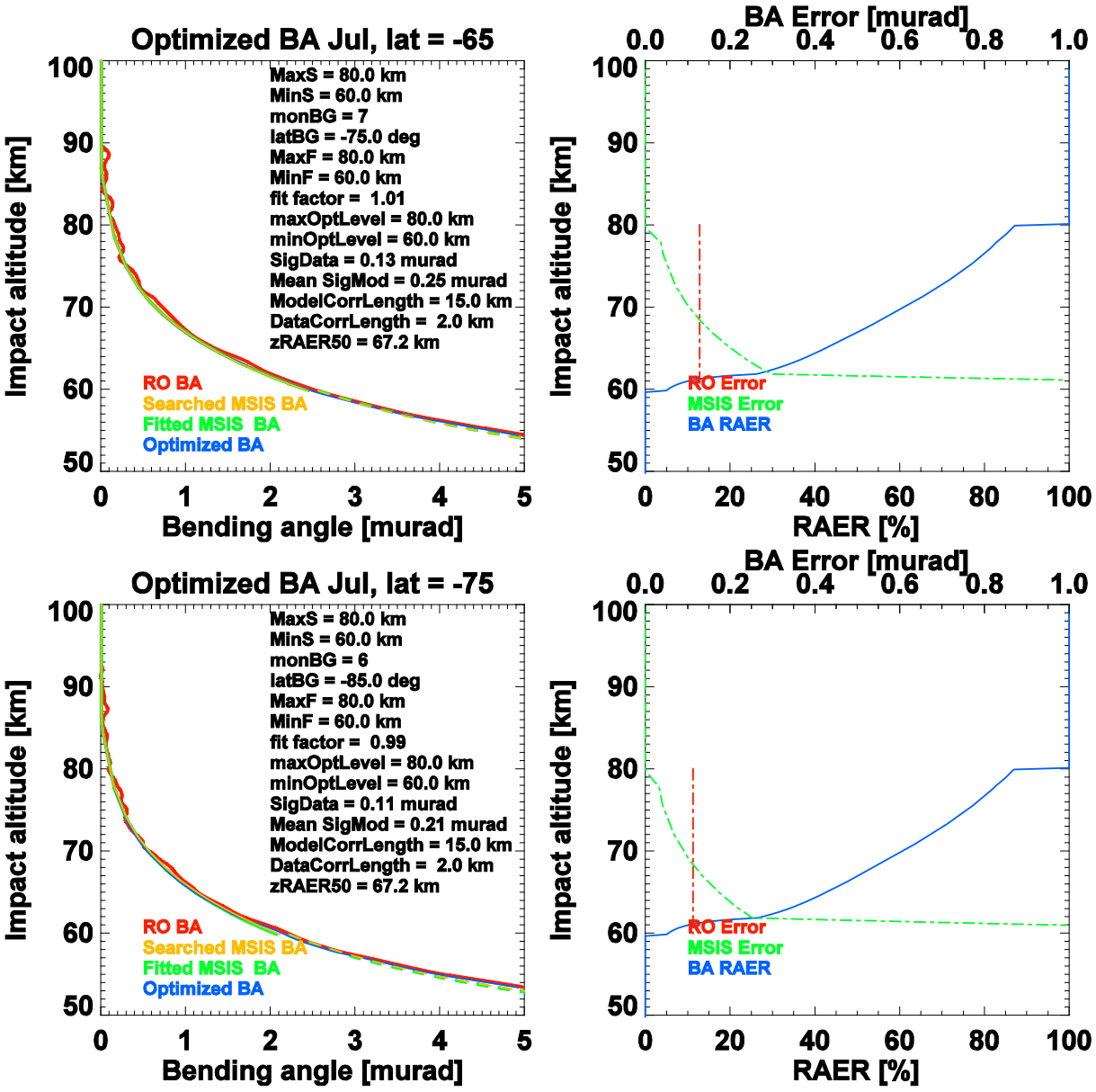

Fig. 8. Statistical optimization of RO bending angles and MSIS background for July within 10° latitude bands from North to South.

3. The BAROCLIM Bending Angle Climatology

3.1 Monthly Mean Bending Angles

Here we finally show the bending angle climatology (BAROCLIM), obtained by statistical optimization of raw bending angle data and MSIS climatology (one bending angle profile per 10° latitude band) for all months of the year (Fig. 8: January to June, Fig. 9: July to December).

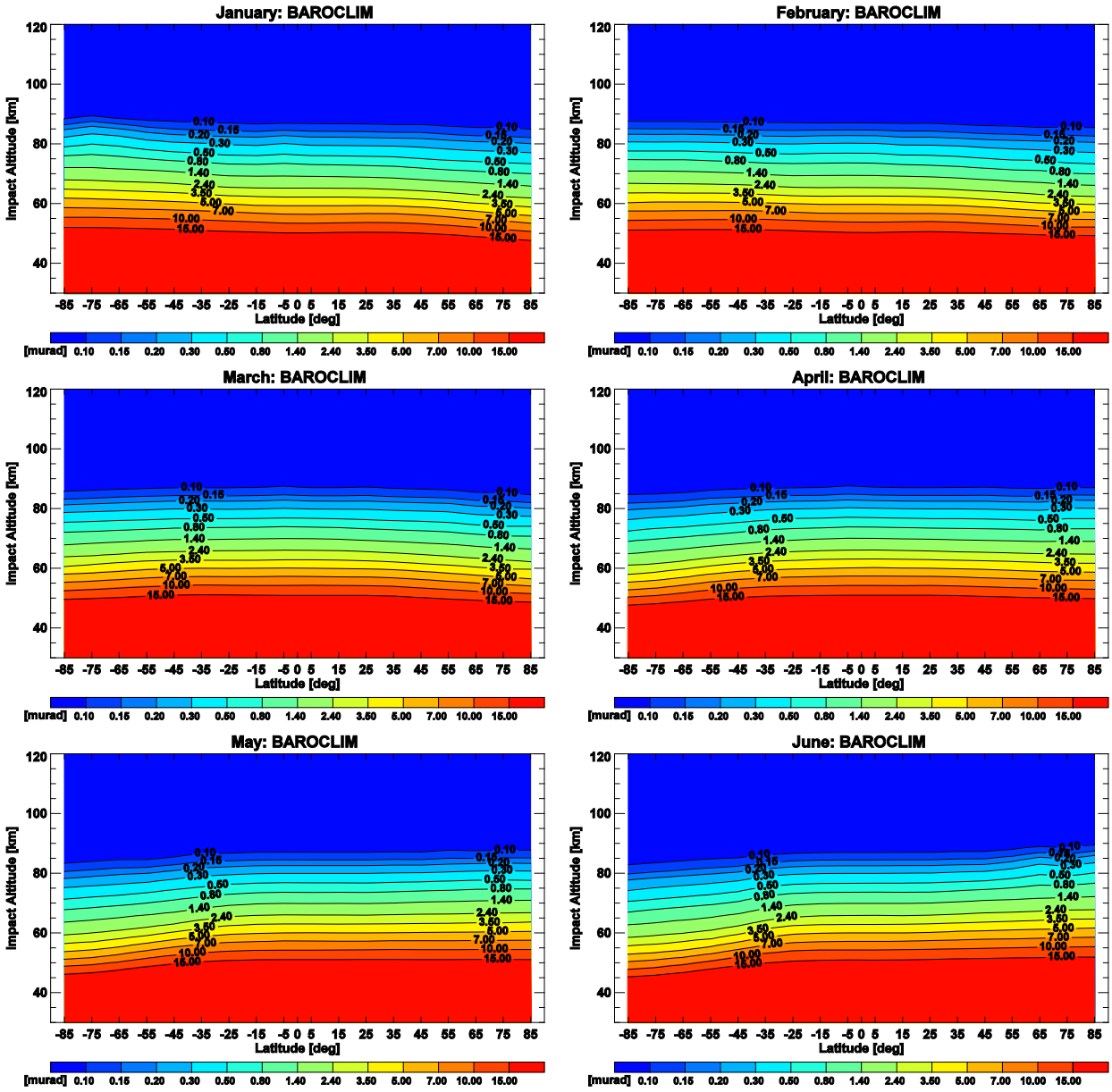

Fig. 8. Statistically optimized bending angle climatologies for the months January to June between 30 km and 120 km impact altitude.

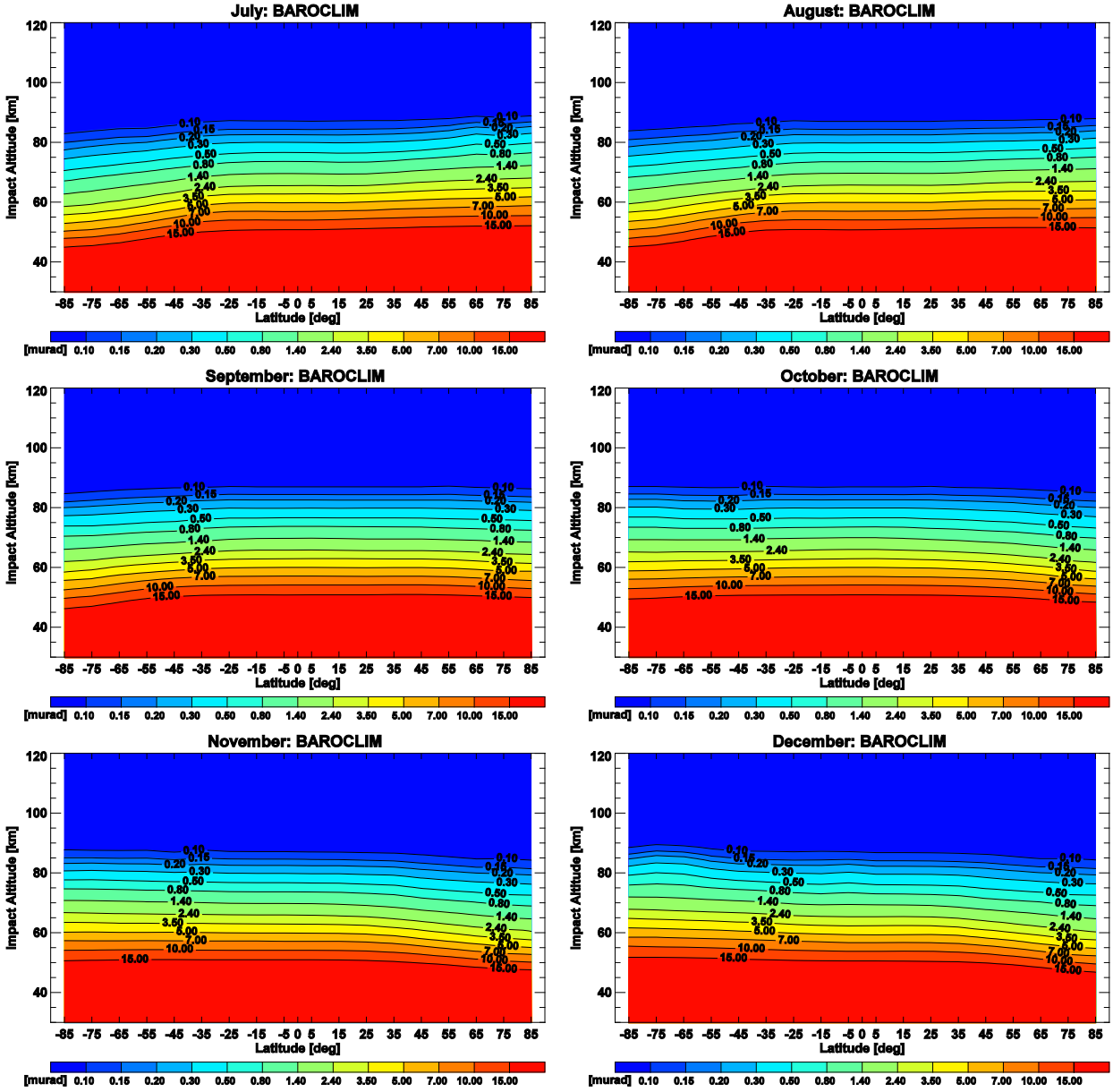

Fig. 9. Statistically optimized bending angle climatologies for the months July to December between 30 km and 120 km impact altitude.

3.2 Differences between BAROCLIM and MSIS

Differences between BAROCLIM and the MSIS climatology illustrate characteristics of the new BAROCLIM climatology. Figure 10 and Fig. 11 show monthly mean (relative) systematic differences between BAROCLIM and the MSIS profiles that would have been used as background by the WEGC standard retrieval in the (operationally not used) MSIS mode (here termed "standard MSIS"). Those profiles are obtained by searching the library for the best fitting MSIS profile in the 35 km to 55 km altitude interval, and fitting it to the RO data between 45 km und 65 km altitude.

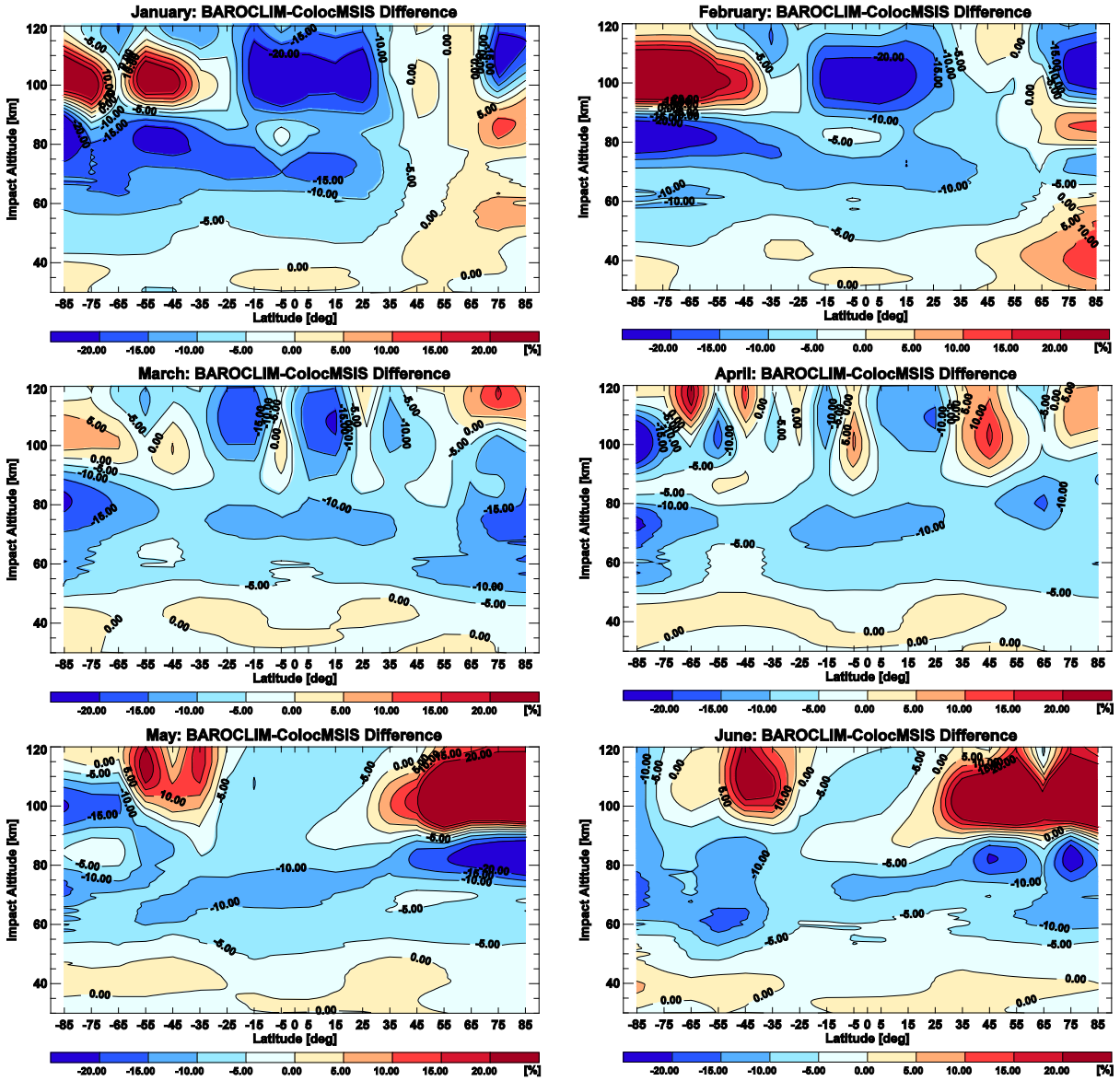

Fig. 10. Systematic difference between BAROCLIM (Fig. 8) and "standard MSIS" climatology for the months January to June, between 30 km and 120 km impact altitude.

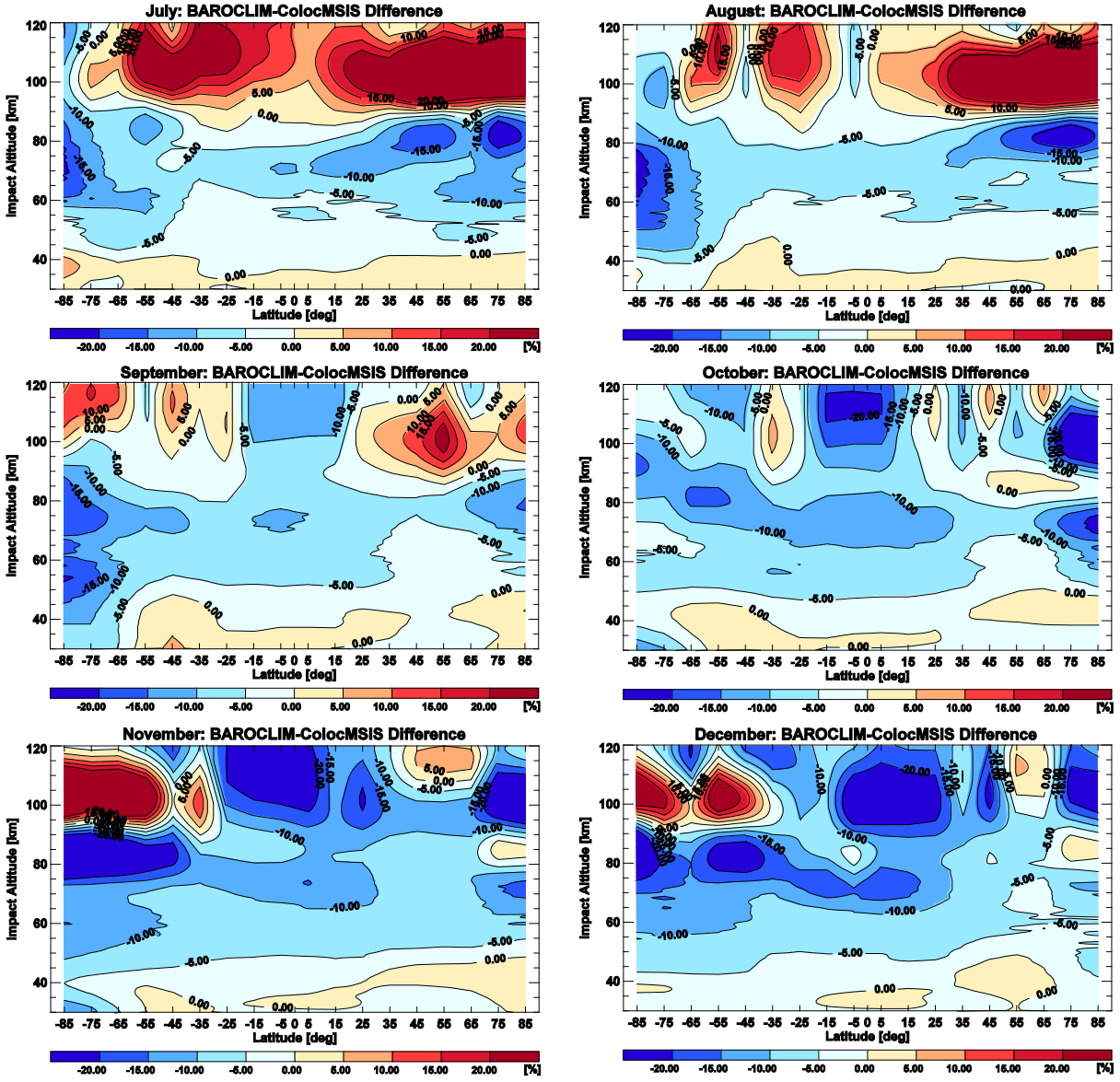

Fig. 11. Systematic difference between BAROCLIM (Fig. 9) and "standard MSIS" climatology for the months July to December, between 30 km and 120 km impact altitude.

"Standard MSIS" bending angles would (by design) provide quite a good fit to RO bending angles – and therefore also to BAROCLIM bending angels up to ~60 km altitude. Between 60 km and 80 km impact altitude, however, they are almost exclusively larger than RO bending angles – and therefore also larger than BAROCLIM bending angels in this altitude range ("blue" areas in Fig. 10 and Fig. 11, respectively).

It is therefore important to employ the search-and-fit procedure (section 2.4) when combining the RO bending angles with MSIS climatology above 60 km altitude, since "standard MSIS" profiles would be systematically biased at theses altitudes.

Figure 12 and Fig. 13 show (relative) systematic differences between BAROCLIM and search-fitted MSIS. The setup of the statistical optimization (section 2.5) ensures, that BAROCLIM bending angles are identical to search-fitted MSIS bending angles at impact altitudes above 80 km – and identical to RO bending angles at impact altitudes below 60 km. Differences are therefore only shown up to 90 km altitudes.

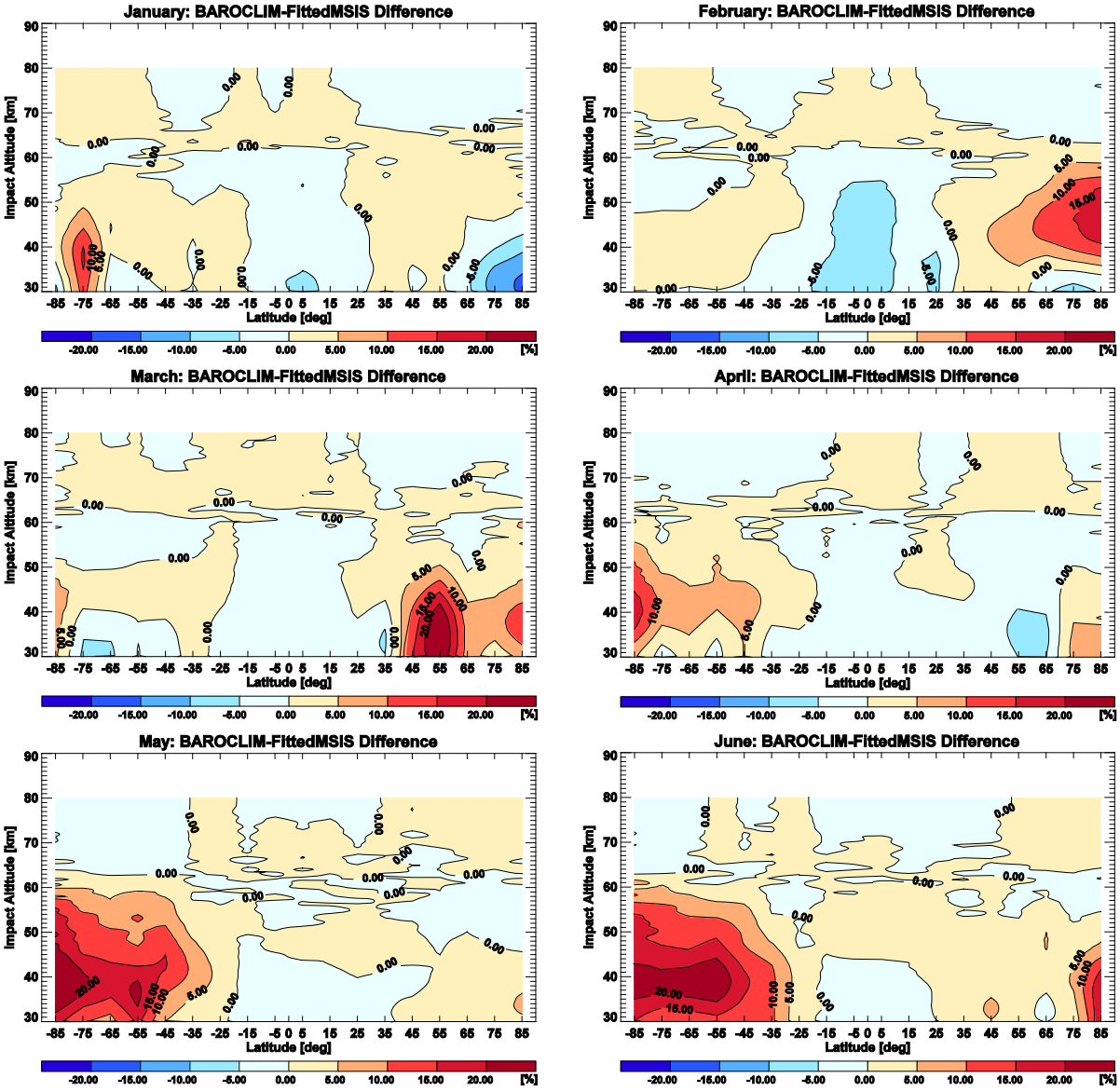

Fig. 12. Systematic difference between BAROCLIM (Fig. 8) and search-fitted MSIS climatology for the months January to June, between 30 km and 90 km impact altitude. Note that differences above 80 km altitude must be zero due to the setup of the statistical optimization (section 2.5).

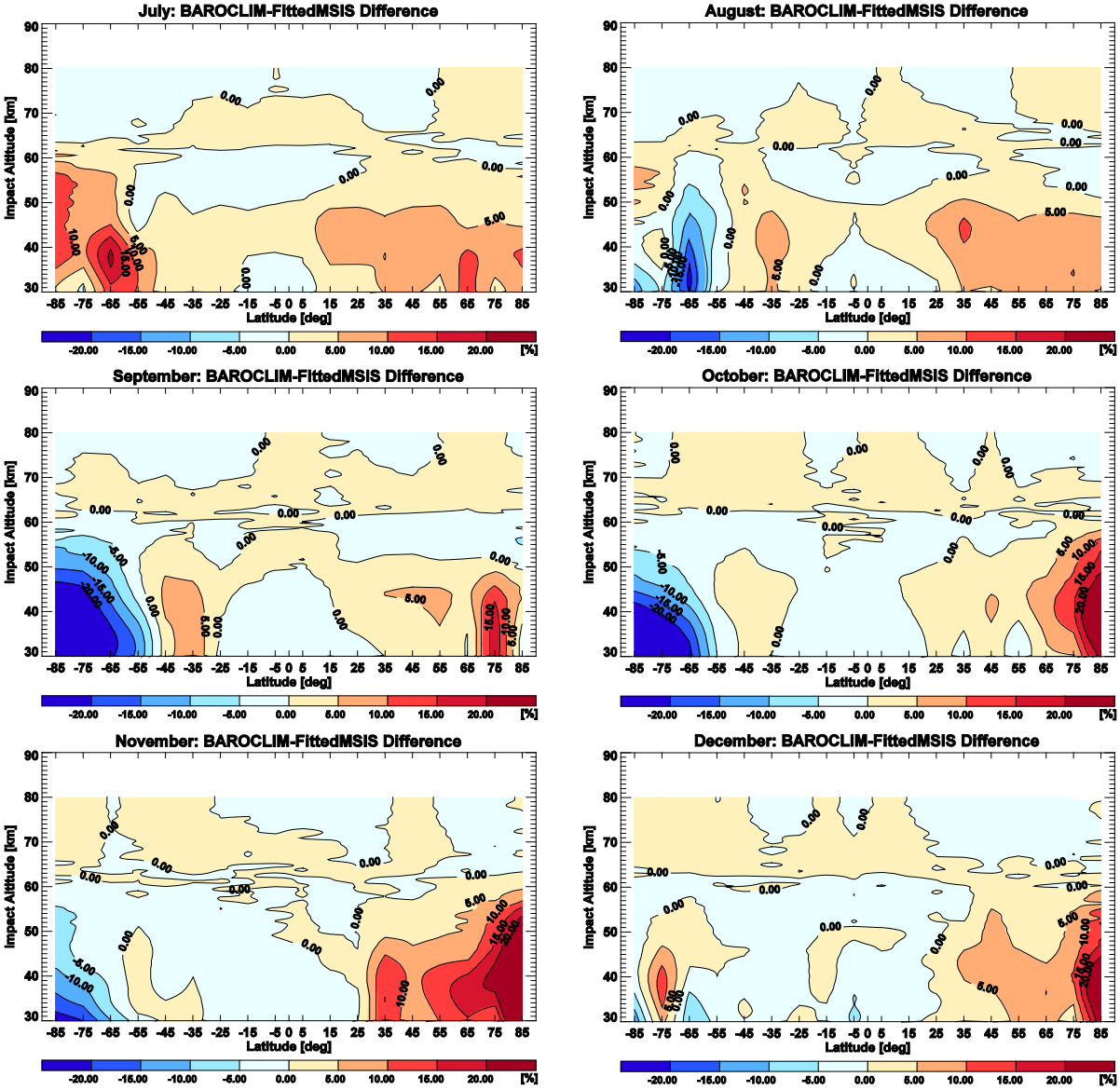

Fig. 13. Systematic difference between BAROCLIM (Fig. 9) and search-fitted MSIS climatology for the months July to December, between 30 km and 90 km impact altitude. Note that differences above 80 km altitude must be zero due to the setup of the statistical optimization (section 2.5).

The search-and-fit procedure (section 2.4) leads to considerably better agreement between background and observations between 60 km and 80 km impact altitude (Fig. 12 and 13, respectively), while larger differences below 60 km do not matter, since MSIS data are not used at all below that altitude (below 60 km BAROCLIM is a pure RO bending angle climatology).

Overall, the difference plots (Fig. 10 to Fig. 13) clearly show that there are considerable differences between the final product, and the MSIS climatology, which has been used as additional background information at altitudes above ~65 km, where even averaged bending angels start being too noise to be used as the only background information source.

3.3 Differences between BAROCLIM and ECMWF

A detailed validation of the BAROCLIM climatology is beyond the scope of the present study (see also challenge 6 in section 1.3.2). Here we show, however, some initial results, based on comparison with co-located ECMWF analyses profiles. Thereby we focus on the impact altitude range from 0 km to 60 km – where BAROCLIM bending angles are identical to averaged F3C RO bending angles (section 2.5). Figure 14 shows the results for January to June, Fig. 15 the respective results for July to December (note the finer contour spacing compared to the previous difference plots).

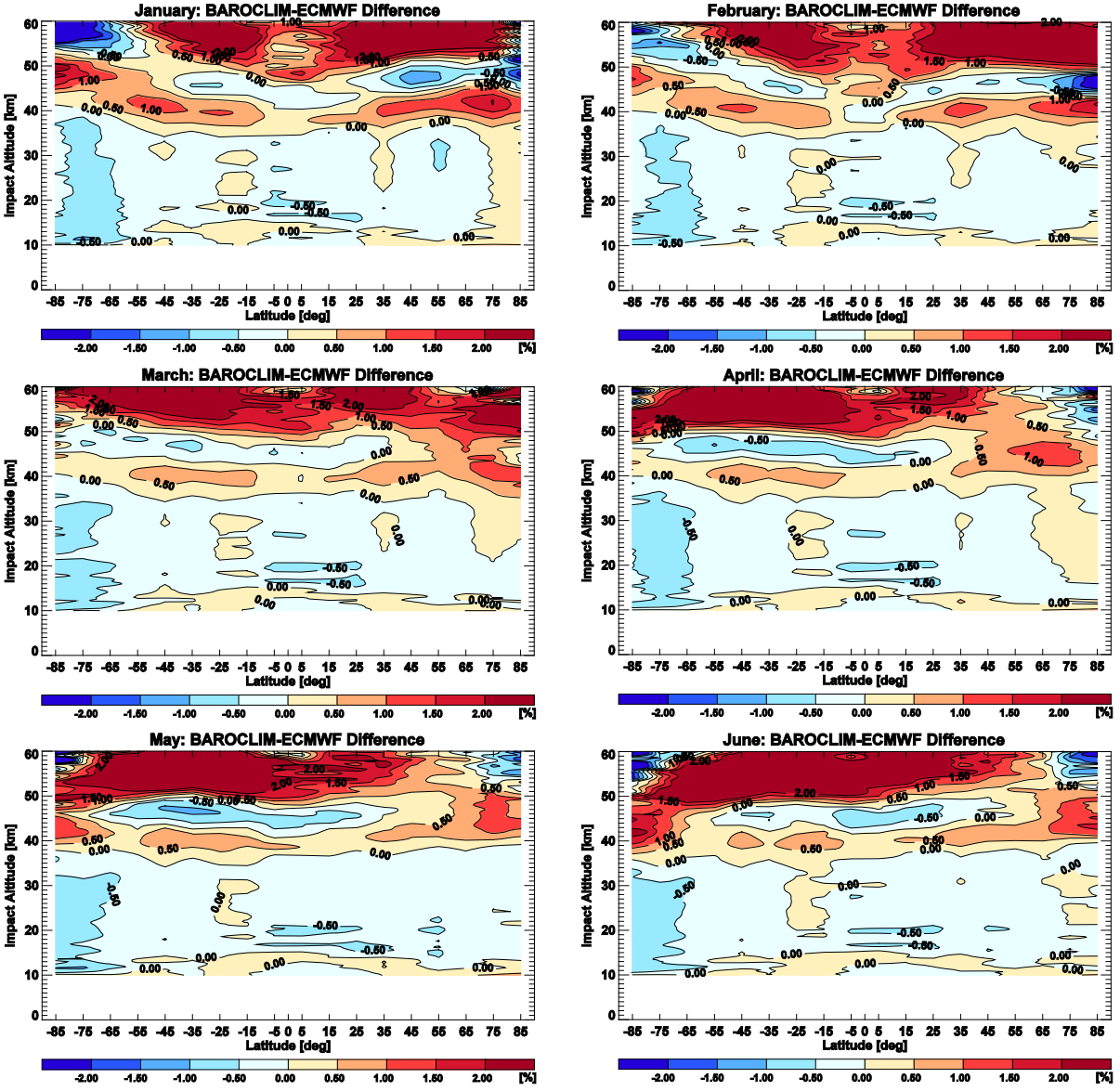

Fig. 14. Systematic difference between BAROCLIM (Fig. 8) and ECMWF analyses for the months January to June between 0 km and 60 km impact altitude.

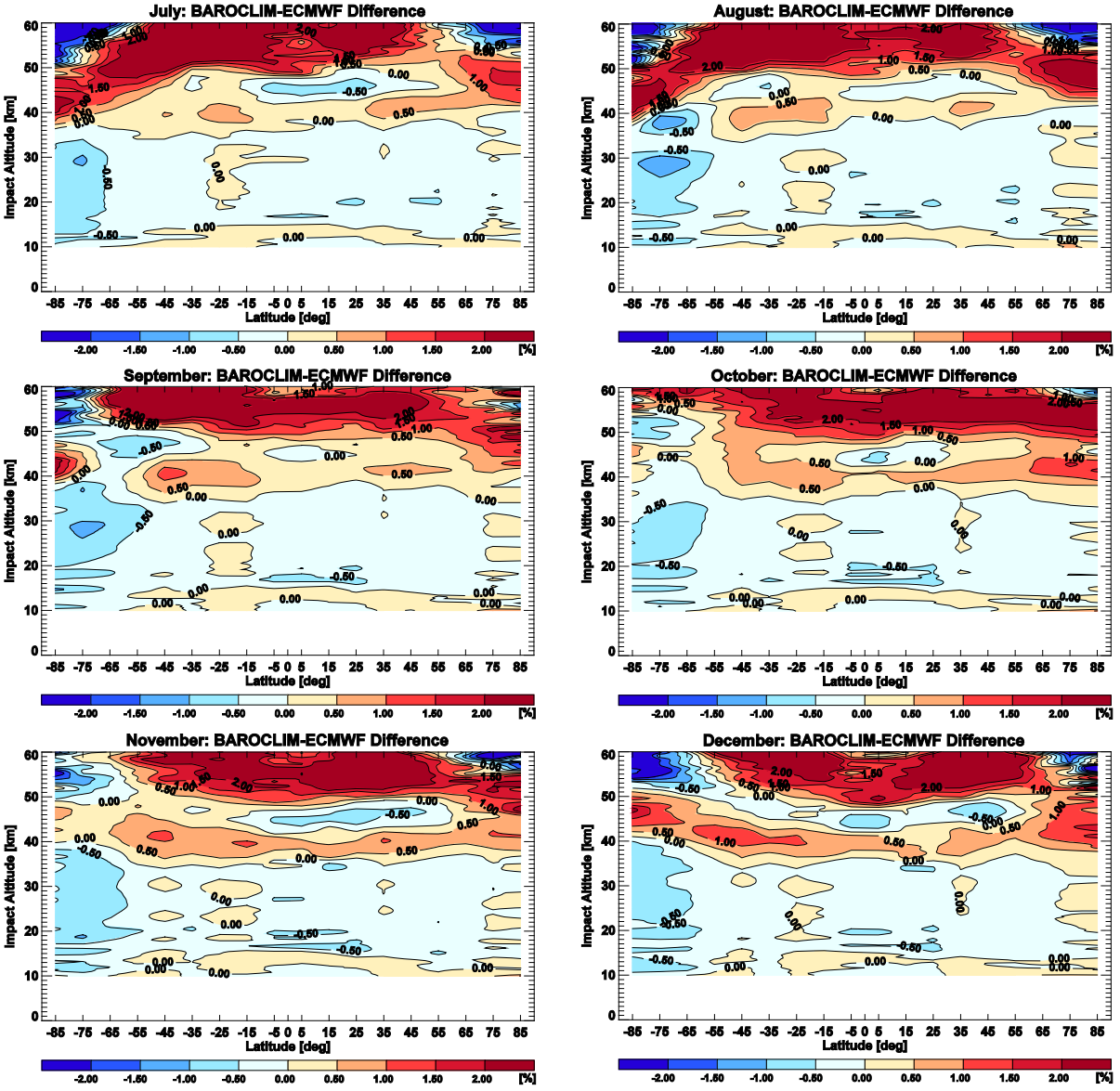

Fig. 15. Systematic difference between BAROCLIM (Fig. 9) and ECMWF analyses for the months July to December between 0 km and 60 km impact altitude.

Both figures show some pertinent features: Relative differences below ~40 km are generally small and seldom exceed 0.5 %, which is not too surprising, since ECMWF assimilates F3C RO data – up to 50 km altitude. Interestingly, right below this altitude is a "band" of positive BAROCLIM – ECMWF differences with values reaching 1.5 % and more. Beyond 50 km we see predominantly positive deviations of more than 2 %.

At least the differences between ~40 km and ~50 km are very likely not caused by errors in the RO data, but by a known bias in ECMWF analyses (Sean Healy, ECMWF, personal communication, 2012).

4. Conclusions

Current Radio Occultation (RO) retrieval schemes use different types of background data for high altitude initialization, which is unavoidable, if RO data beyond bending angle level are desired. These background data range from exponential extrapolation of the bending angle profile via climatologies to NWP (Numerical Weather Prediction) short-term forecast data. Each approach has advantages but also shortcomings, leading to considerable differences between higher-level RO data from different processing centers. Large biases in the employed high-altitude (above ~30 km) background data lead to notable biases in RO data also at lower altitudes (below ~30 km), due to the downward propagation of errors when performing the Abel integral and the hydrostatic integral. Unbiased high-altitude data would therefore be very valuable, in order to extend the vertical domain, where derived RO data can still be safely used.

We tested a new approach, based on the assumption that RO data at altitudes above ~50 km altitude, which are generally too noisy to be used as individual profiles, are still valuable (and largely unbiased), as long as averages over many RO profiles are considered. We found that data from F3C (COSMIC) have sufficient quality for this purpose. The data employed – from August 2006 until July 2011 – have been furthermore gathered in years with low solar activity. The risk of possible contamination due to un-corrected ionospheric errors is therefore low.

We had to perform a reprocessing to obtain the required raw bending angle data, applied a simple, twofold outlier rejection scheme, and tested different ways to combine the new bending angle climatology with additional background information, which is still needed at (even) higher altitudes. Statistical optimization delivers mean bending angle profiles (BAROCLIM), which are reasonably smooth, and make optimal use of the (still) high RO data quality at altitudes between ~50 km and up to ~75 km (where individual profiles are usually not used anymore). Above 80 km BAROCLIM profiles are identical to MSIS climatology profiles, which have been found best-fitting after library search and application of a fitting factor. BAROCLIM is available in NetCDF format, as monthly mean bending angle profiles per 10° latitude bands. We are confident that BAROCLIM will be at least of similar usefulness as the climatologies that are currently used for high-altitude bending angle initialization.

Acknowledgments

The authors would like to thank Kent B. Lauritsen and Stig Syndergaard (GRAS-SAF/ROM-SAF and DMI, Copenhagen, Denmark) for the invitation to perform this visiting scientist study, for scientific discussion and advice. The Pre-existing software and databases used in this study were provided by Wegener Center for Climate and Global Change and funded by the Austrian Science Fund (FWF; BENCHCLIM project P22293-N21).

References

Ao, C. O., A. J. Mannucci,, and E. R. Kursinski (2012), Improving GPS Radio occultation stratospheric refractivity retrievals for climate benchmarking, *Geophys. Res. Lett.*, 39, L12701, doi:10.1029/2012GL051720.

Danzer, J., B. Scherllin-Pirscher, and U. Foelsche (2012), Systematic residual ionospheric error in radio occultation data, *Geophysical Research Abstracts*, Vol. 14, EGU2012-9845, 2012.

Fjeldbo, G., A.J. Kliore, and V. Eshleman (1971), The neutral atmosphere of Venus as studied with Mariner V radio occultation experiments, *Astron. J.*, 76, 123–140, doi:10.1086/111096.

Foelsche, U., G. Kirchengast, A.K. Steiner, L. Kornblueh, E. Manzini, and L. Bengtsson (2008), An observing system simulation experiment for climate monitoring with GNSS radio occultation data: Setup and test bed study. *J. Geophys. Res.*, 113, D11108, doi:10.1029/2007JD009231.

Foelsche, U., B. Pirscher, M. Borsche, G. Kirchengast, and J. Wickert (2009), Assessing the Climate Monitoring Utility of Radio Occultation Data: From CHAMP to FORMOSAT-3/COSMIC, *Terr. Atmos. Oceanic Sci.*, 20, 155–170, doi: 10.3319/TAO.2008.01.14.01(F3C).

Foelsche, U., B. Scherllin-Pirscher, F. Ladstädter, A.K. Steiner, and G. Kirchengast (2011), Refractivity and temperature climate records from multiple radio occultation satellites consistent within 0.05%, *Atmos. Meas. Tech.*, 4, 2007–2018, doi:10.5194/amt-4-2007-2011.

Gleisner, H., and S. B. Healy (2012), A simplified approach for generating GNSS radio occultation refractivity climatologies, *Atmos. Meas. Tech. Disc.*, 5, 5245-5269, doi:10.5194/amtd-5-5245-2012

Healy, S.B. (2001), Radio occultation bending angle and impact parameter errors caused by horizontal refractive index gradients in the troposphere: A simulation study, *J. Geophys. Res.*, 106, 11875–11889.

Hedin, A.E. (1991), Extension of the MSIS thermosphere model into the middle and lower atmosphere, *J. Geophys. Res.*, 96, 1159–1172.

Ho, S.-P., G. Kirchengast, S. Leroy, J. Wickert, T. Mannucci, A.K. Steiner, D. Hunt, W. Schreiner, S.V. Sokolovskiy, C.O. Ao, M. Borsche, A. von Engeln, U. Foelsche, S. Heise, B. Iijima, Y.-H. Kuo, E.R. Kursinski, B. Pirscher, M. Ringer, C. Rocken, and T. Schmidt (2009), Estimating the uncertainty of using GPS radio occultation data for climate monitoring: Inter-comparison of CHAMP refractivity climate records 2002 to 2006 from different data centers, *J. Geophys. Res.*, 114, D23107, doi:10.1029/2009JD011969.

Ho, S.-P., D. Hunt, A.K. Steiner, A. Mannucci, G. Kirchengast, H. Gleisner, S. Heise, A. von Engeln, C. Marquardt, S. Sokolovskiy, W. Schreiner, B. Scherllin-Pirscher, C. Ao, J. Wickert, S. Syndergaard, K. Lauritsen, S. Leroy, E.R. Kursinski, Y.-H. Kuo, U. Foelsche, T. Schmidt, M. Gorbunov (2012), Reproducibility of GPS Radio Occultation Data for Climate Monitoring: Profile-to-Profile Inter-comparison of CHAMP Climate Records 2002 to 2008 from Six Data Centers, *J. Geophys. Res.*, revised, 2012

Kursinski, E.R., G.A. Hajj, K.R. Hardy, J.T. Schofield, and R. Linfield (1997), Observing the Earth's atmosphere with radio occultation measurements using the Global Positioning System, *J. Geophys. Res.*, 102, 23429–23465.

Pirscher, B. (2010), Multi-Satellite Climatologies of Fundamental Atmospheric Variables From Radio Occultation and Their Validation, *Ph.D. thesis*, Wegener Center Verlag Graz, Sci. Rep. 33-2010.

Rieder, M.J., and G. Kirchengast (2001), Error analysis and characterization of atmospheric profiles retrieved from GNSS occultation data, *J. Geophys. Res.*, 106, 31755-31770.

Schreiner, W., Y.-H. Kuo, S.-P. Ho, S. Sokolovskiy, and D. Hunt (2011), Use of GNSS radio occultation data for climate monitoring and trend detection, poster at the World Climate Research Program (WCRP) conference, session C23.

Steiner, A.K., D. Hunt, S.-P. Ho, G. Kirchengast, A.J. Mannucci, B. Scherllin-Pirscher, H. Gleisner, A. von Engeln, T. Schmidt, C. Ao, S.S. Leroy, E.R. Kursinski, U. Foelsche, M. Gorbunov, Y.-H. Kuo, K.B. Lauritsen, C. Marquardt, C. Rocken, W. Schreiner, S. Sokolovskiy, S. Syndergaard, S. Heise, and J. Wickert (2012), Quantification of Structural Uncertainty in Climate Data Records from GPS Radio Occultation, *J. Geophys. Res*., revised, 2012

List of Acronyms

BAROCLIM	Bending Angle Radio Occultation Climatology
CHAMP	CHAllenging Minisatellite Payload
CLIPS	Climatology Processing System, software tool at WEGC
COSMIC	Constellation Observing System for Meteorology, Ionosphere, and Climate
ECMWF	European Centre for Medium-range Weather Forecasts
EUMETSAT	EUropean organisation for the exploitation of METeorological SATellites
F3C	FORMOSAT-3/COSMIC
FORMOSAT-3	Formosa Satellite Mission 3
FM	Flight Model (1 – 6) of the F3C constellation
GNSS	Global Navigation Satellite System (generic term e.g., for GPS, GALILEO)
GPS	Global Positioning System (USA)
GRAS	GNSS Receiver for Atmospheric Sounding (on Metop)
GRAS SAF	EUMETSAT's GRAS Satellite Application Facility
IGAM	Institute for Geophysics, Astrophysics, and Meteorology, UniGraz
Metop	Meteorological Operational Satellite
MSIS	Mass Spectrometer and Incoherent Scatter Radar [model of the middle atmosphere]
NetCDF	Network Common Data Form
NWP	Numerical Weather Prediction
RO	Radio Occultation
SO	Statistical Optimization
SSW	Sudden Stratospheric Warming
UniGraz	University of Graz, Austria
UCAR	University Corporation for Atmospheric Research (USA)
WEGC	Wegener Center for Climate and Global Change, UniGraz

Appendix A: Statistical Optimization Results for January, April, and October

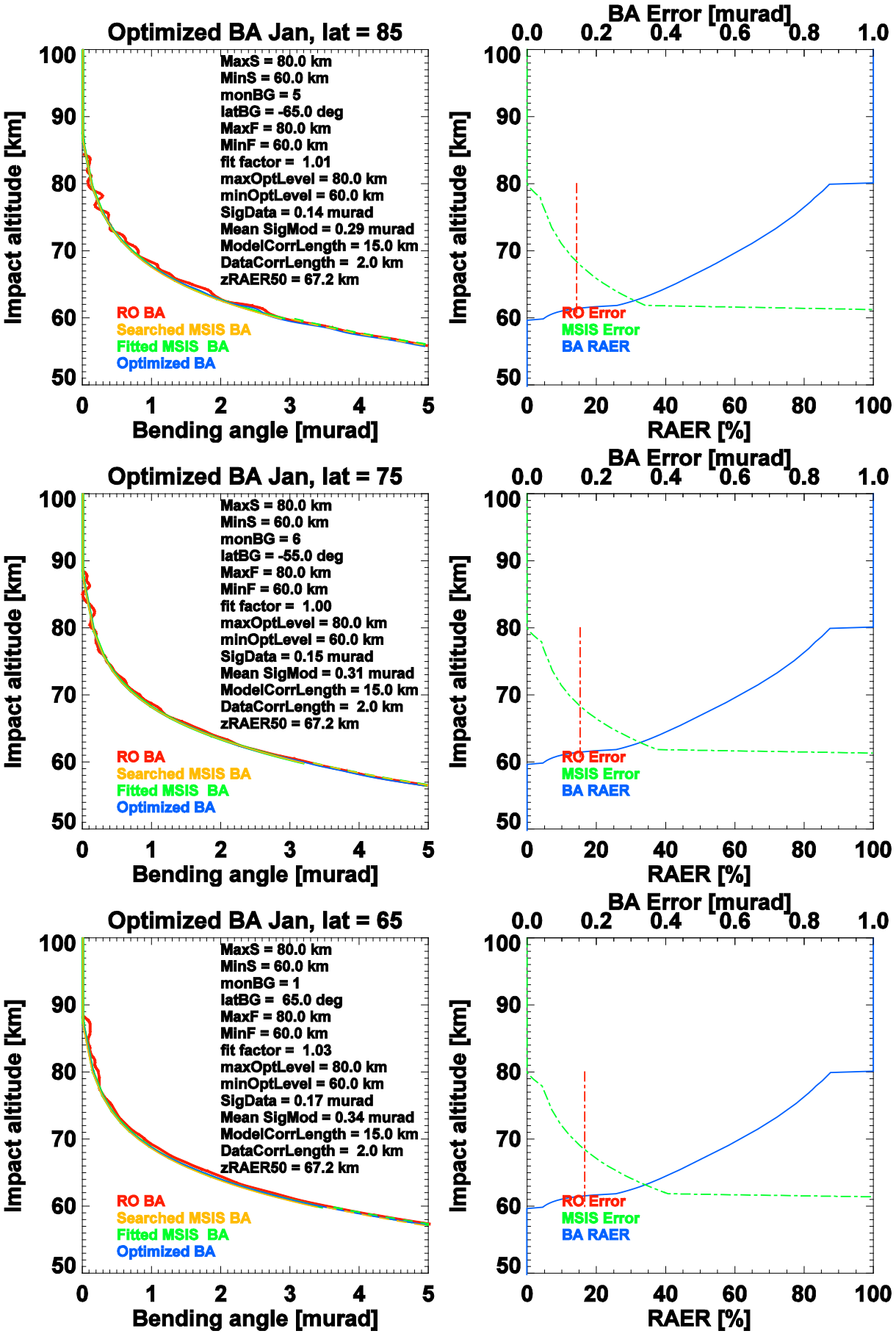
Optimized BA Jan, lat = 85
MaxS = 80.0 km
MinS = 60.0 km
monBG = 5
latBG = -65.0 deg
MaxF = 80.0 km
MinF = 60.0 km
fit factor = 1.01
maxOptLevel = 80.0 km
minOptLevel = 60.0 km
SigData = 0.14 murad
Mean SigMod = 0.29 murad
ModelCorrLength = 15.0 km
DataCorrLength = 2.0 km
zRAER50 = 67.2 km
RO BA
Searched MSIS BA
Fitted MSIS BA
Optimized BA
Impact altitude [km]
Bending angle [murad]
BA Error [murad]
RO Error
MSIS Error
BA RAER
RAER [%]
Optimized BA Jan, lat = 75
MaxS = 80.0 km
MinS = 60.0 km
monBG = 6
latBG = -55.0 deg
MaxF = 80.0 km
MinF = 60.0 km
fit factor = 1.00
maxOptLevel = 80.0 km
minOptLevel = 60.0 km
SigData = 0.15 murad
Mean SigMod = 0.31 murad
ModelCorrLength = 15.0 km
DataCorrLength = 2.0 km
zRAER50 = 67.2 km
Optimized BA Jan, lat = 65
MaxS = 80.0 km
MinS = 60.0 km
monBG = 1
latBG = 65.0 deg
MaxF = 80.0 km
MinF = 60.0 km
fit factor = 1.03
maxOptLevel = 80.0 km
minOptLevel = 60.0 km
SigData = 0.17 murad
Mean SigMod = 0.34 murad
ModelCorrLength = 15.0 km
DataCorrLength = 2.0 km
zRAER50 = 67.2 km

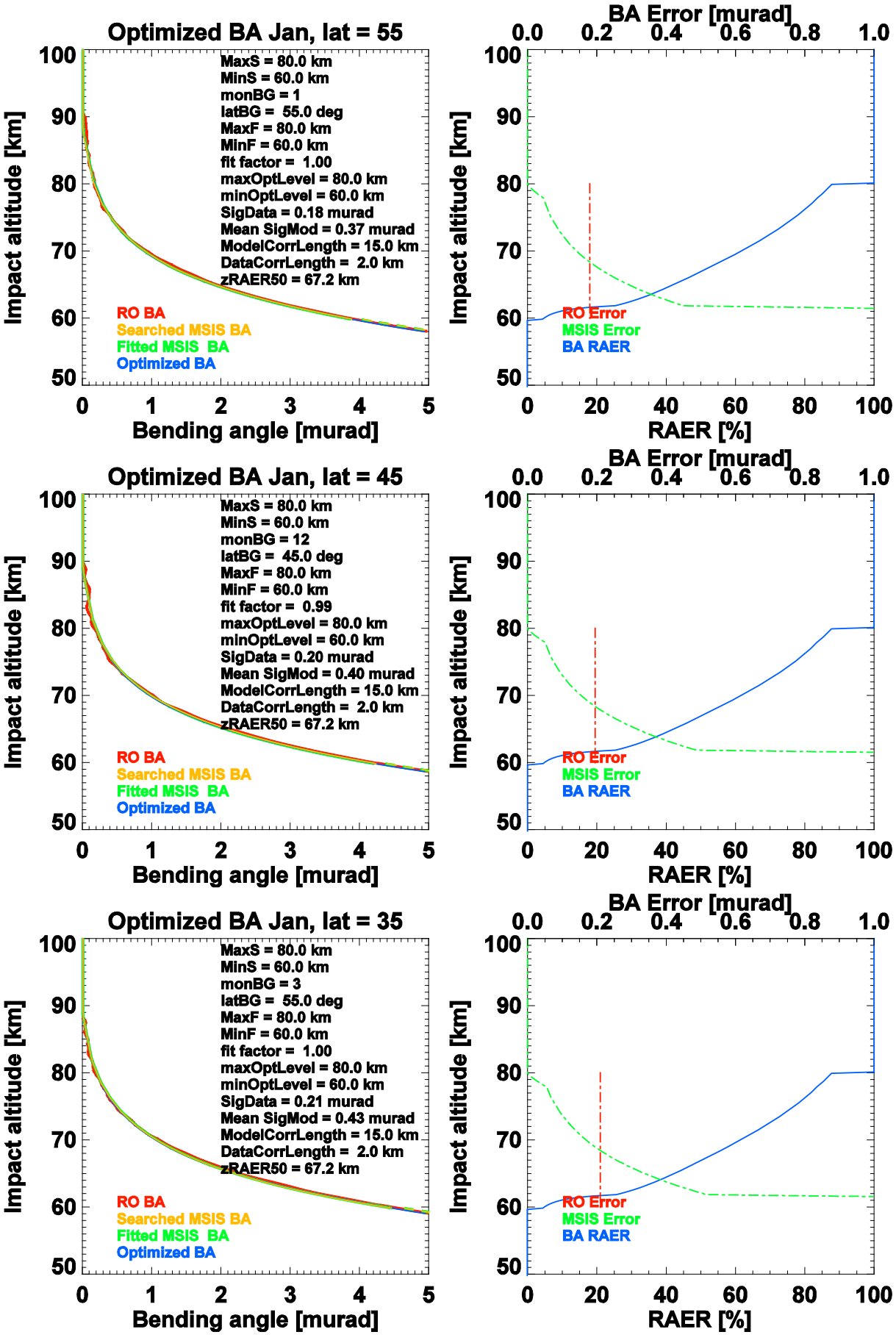
Optimized BA Jan, lat = 55
MaxS = 80.0 km
MinS = 60.0 km
monBG = 1
latBG = 55.0 deg
MaxF = 80.0 km
MinF = 60.0 km
fit factor = 1.00
maxOptLevel = 80.0 km
minOptLevel = 60.0 km
SigData = 0.18 murad
Mean SigMod = 0.37 murad
ModelCorrLength = 15.0 km
DataCorrLength = 2.0 km
zRAER50 = 67.2 km
RO BA
Searched MSIS BA
Fitted MSIS BA
Optimized BA
Impact altitude [km]
Bending angle [murad]
BA Error [murad]
RO Error
MSIS Error
BA RAER
RAER [%]
Optimized BA Jan, lat = 45
MaxS = 80.0 km
MinS = 60.0 km
monBG = 12
latBG = 45.0 deg
MaxF = 80.0 km
MinF = 60.0 km
fit factor = 0.99
maxOptLevel = 80.0 km
minOptLevel = 60.0 km
SigData = 0.20 murad
Mean SigMod = 0.40 murad
ModelCorrLength = 15.0 km
DataCorrLength = 2.0 km
zRAER50 = 67.2 km
Optimized BA Jan, lat = 35
MaxS = 80.0 km
MinS = 60.0 km
monBG = 3
latBG = 55.0 deg
MaxF = 80.0 km
MinF = 60.0 km
fit factor = 1.00
maxOptLevel = 80.0 km
minOptLevel = 60.0 km
SigData = 0.21 murad
Mean SigMod = 0.43 murad
ModelCorrLength = 15.0 km
DataCorrLength = 2.0 km
zRAER50 = 67.2 km

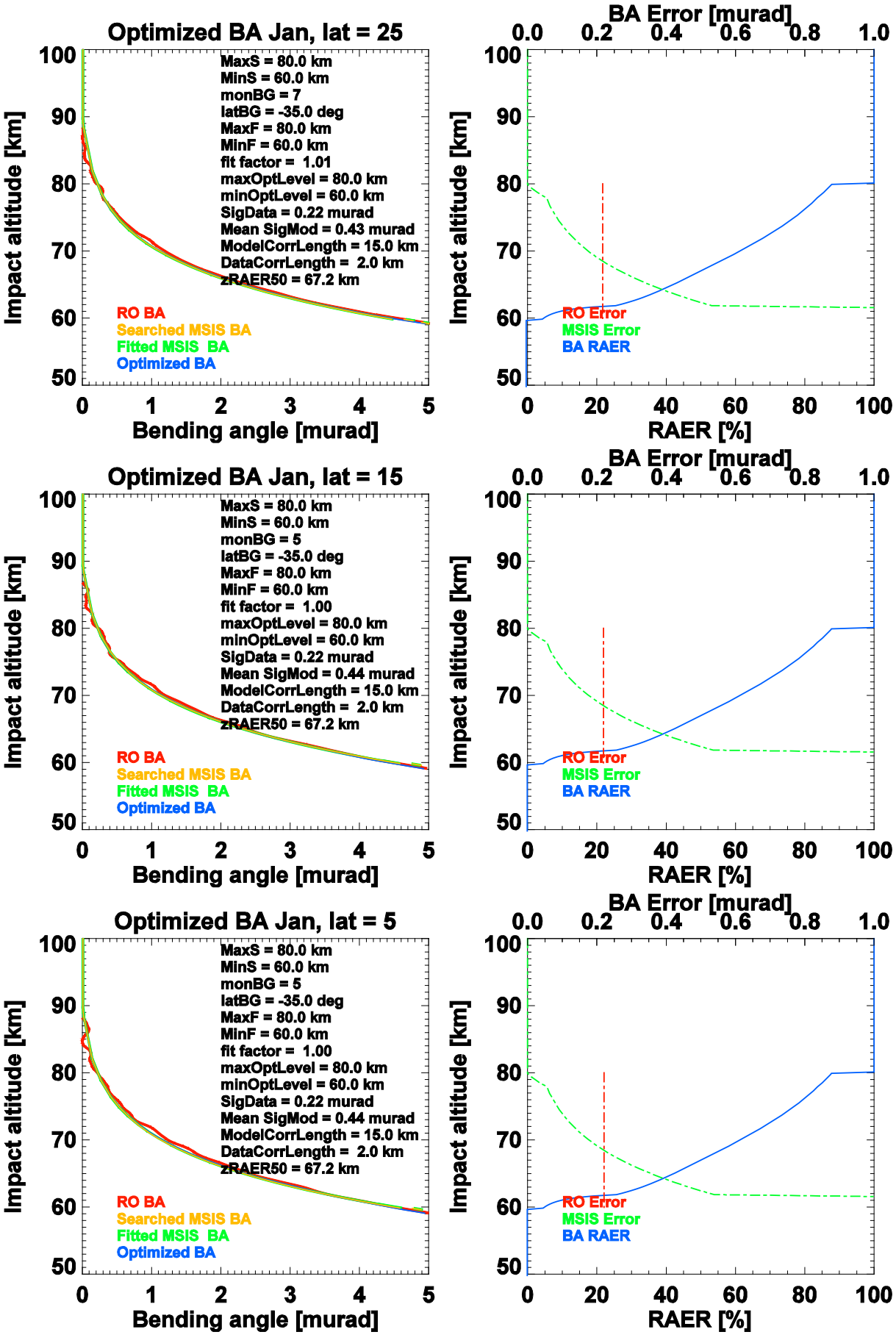
Optimized BA Jan, lat = 25
MaxS = 80.0 km
MinS = 60.0 km
monBG = 7
latBG = -35.0 deg
MaxF = 80.0 km
MinF = 60.0 km
fit factor = 1.01
maxOptLevel = 80.0 km
minOptLevel = 60.0 km
SigData = 0.22 murad
Mean SigMod = 0.43 murad
ModelCorrLength = 15.0 km
DataCorrLength = 2.0 km
zRAER50 = 67.2 km
RO BA
Searched MSIS BA
Fitted MSIS BA
Optimized BA
Impact altitude [km]
Bending angle [murad]
BA Error [murad]
RO Error
MSIS Error
BA RAER
RAER [%]
Optimized BA Jan, lat = 15
MaxS = 80.0 km
MinS = 60.0 km
monBG = 5
latBG = -35.0 deg
MaxF = 80.0 km
MinF = 60.0 km
fit factor = 1.00
maxOptLevel = 80.0 km
minOptLevel = 60.0 km
SigData = 0.22 murad
Mean SigMod = 0.44 murad
ModelCorrLength = 15.0 km
DataCorrLength = 2.0 km
zRAER50 = 67.2 km
Optimized BA Jan, lat = 5
MaxS = 80.0 km
MinS = 60.0 km
monBG = 5
latBG = -35.0 deg
MaxF = 80.0 km
MinF = 60.0 km
fit factor = 1.00
maxOptLevel = 80.0 km
minOptLevel = 60.0 km
SigData = 0.22 murad
Mean SigMod = 0.44 murad
ModelCorrLength = 15.0 km
DataCorrLength = 2.0 km
zRAER50 = 67.2 km

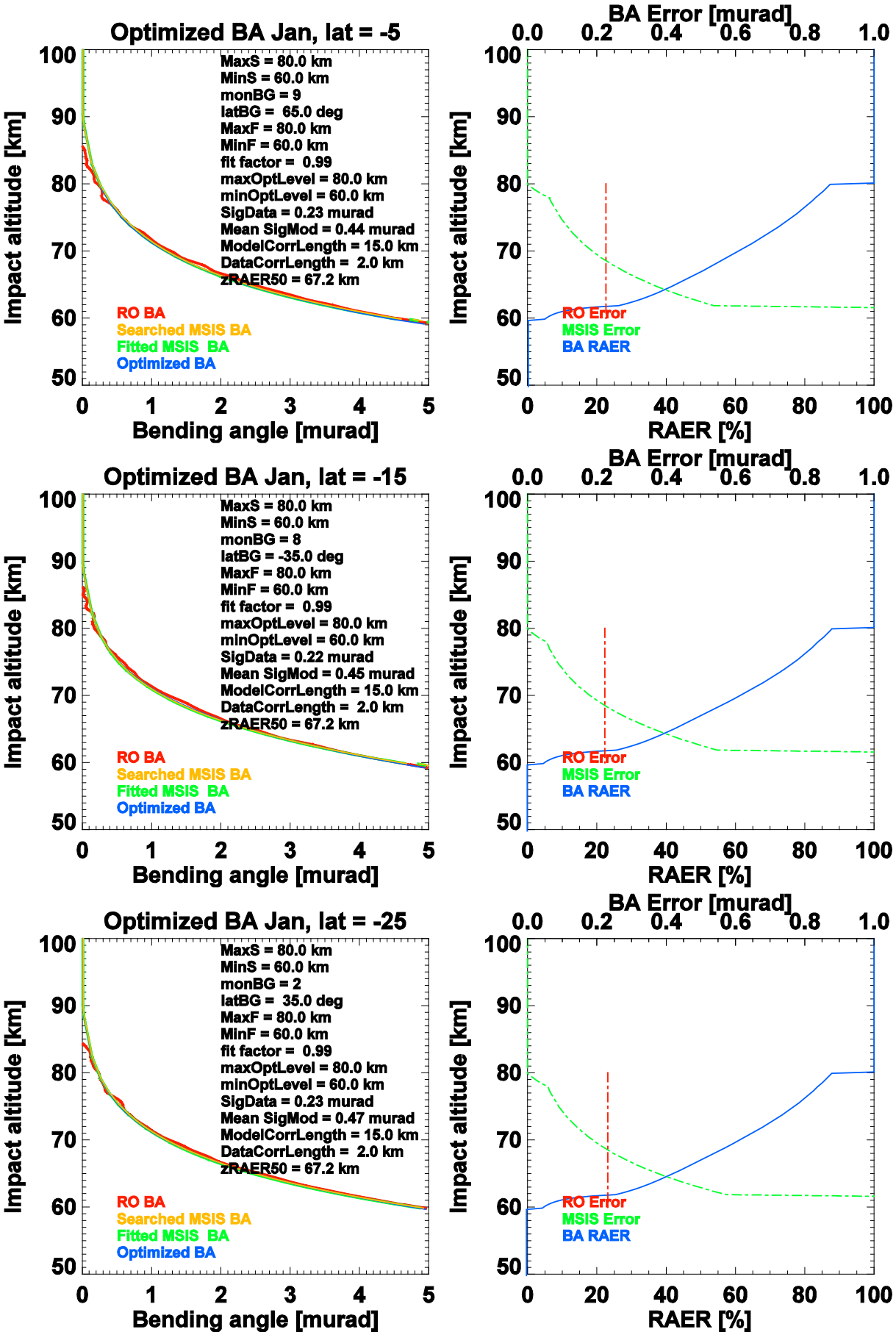
Optimized BA Jan, lat = -5
MaxS = 80.0 km
MinS = 60.0 km
monBG = 9
latBG = 65.0 deg
MaxF = 80.0 km
MinF = 60.0 km
fit factor = 0.99
maxOptLevel = 80.0 km
minOptLevel = 60.0 km
SigData = 0.23 murad
Mean SigMod = 0.44 murad
ModelCorrLength = 15.0 km
DataCorrLength = 2.0 km
zRAER50 = 67.2 km
RO BA
Searched MSIS BA
Fitted MSIS BA
Optimized BA
Impact altitude [km]
Bending angle [murad]
BA Error [murad]
RO Error
MSIS Error
BA RAER
RAER [%]
Optimized BA Jan, lat = -15
MaxS = 80.0 km
MinS = 60.0 km
monBG = 8
latBG = -35.0 deg
MaxF = 80.0 km
MinF = 60.0 km
fit factor = 0.99
maxOptLevel = 80.0 km
minOptLevel = 60.0 km
SigData = 0.22 murad
Mean SigMod = 0.45 murad
ModelCorrLength = 15.0 km
DataCorrLength = 2.0 km
zRAER50 = 67.2 km
RO BA
Searched MSIS BA
Fitted MSIS BA
Optimized BA
Impact altitude [km]
Bending angle [murad]
BA Error [murad]
RO Error
MSIS Error
BA RAER
RAER [%]
Optimized BA Jan, lat = -25
MaxS = 80.0 km
MinS = 60.0 km
monBG = 2
latBG = 35.0 deg
MaxF = 80.0 km
MinF = 60.0 km
fit factor = 0.99
maxOptLevel = 80.0 km
minOptLevel = 60.0 km
SigData = 0.23 murad
Mean SigMod = 0.47 murad
ModelCorrLength = 15.0 km
DataCorrLength = 2.0 km
zRAER50 = 67.2 km
RO BA
Searched MSIS BA
Fitted MSIS BA
Optimized BA
Impact altitude [km]
Bending angle [murad]
BA Error [murad]
RO Error
MSIS Error
BA RAER
RAER [%]

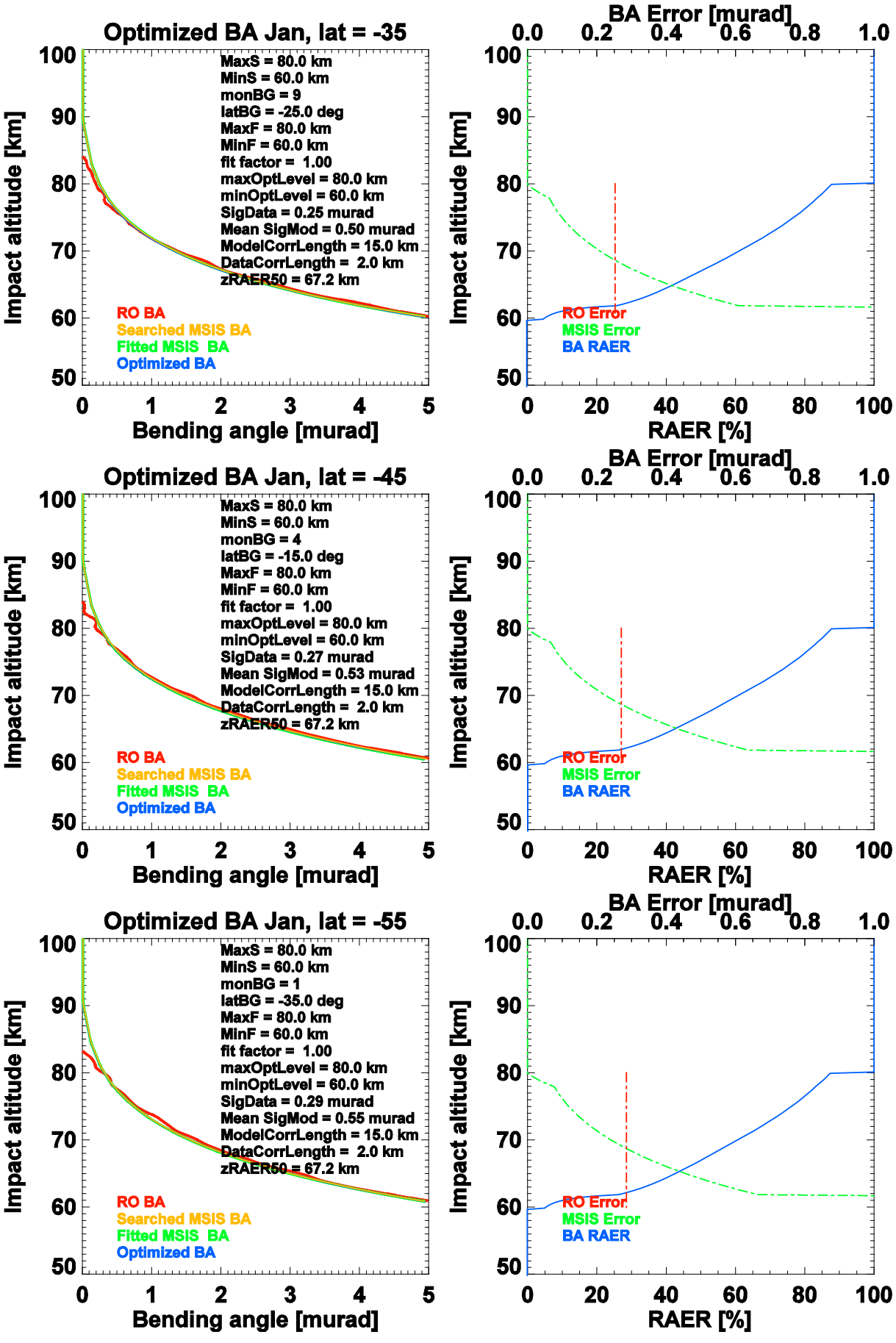
Optimized BA Jan, lat = -35
MaxS = 80.0 km
MinS = 60.0 km
monBG = 9
latBG = -25.0 deg
MaxF = 80.0 km
MinF = 60.0 km
fit factor = 1.00
maxOptLevel = 80.0 km
minOptLevel = 60.0 km
SigData = 0.25 murad
Mean SigMod = 0.50 murad
ModelCorrLength = 15.0 km
DataCorrLength = 2.0 km
zRAER50 = 67.2 km
RO BA
Searched MSIS BA
Fitted MSIS BA
Optimized BA
Impact altitude [km]
Bending angle [murad]
BA Error [murad]
RO Error
MSIS Error
BA RAER
RAER [%]
Optimized BA Jan, lat = -45
MaxS = 80.0 km
MinS = 60.0 km
monBG = 4
latBG = -15.0 deg
MaxF = 80.0 km
MinF = 60.0 km
fit factor = 1.00
maxOptLevel = 80.0 km
minOptLevel = 60.0 km
SigData = 0.27 murad
Mean SigMod = 0.53 murad
ModelCorrLength = 15.0 km
DataCorrLength = 2.0 km
zRAER50 = 67.2 km
Optimized BA Jan, lat = -55
MaxS = 80.0 km
MinS = 60.0 km
monBG = 1
latBG = -35.0 deg
MaxF = 80.0 km
MinF = 60.0 km
fit factor = 1.00
maxOptLevel = 80.0 km
minOptLevel = 60.0 km
SigData = 0.29 murad
Mean SigMod = 0.55 murad
ModelCorrLength = 15.0 km
DataCorrLength = 2.0 km
zRAER50 = 67.2 km

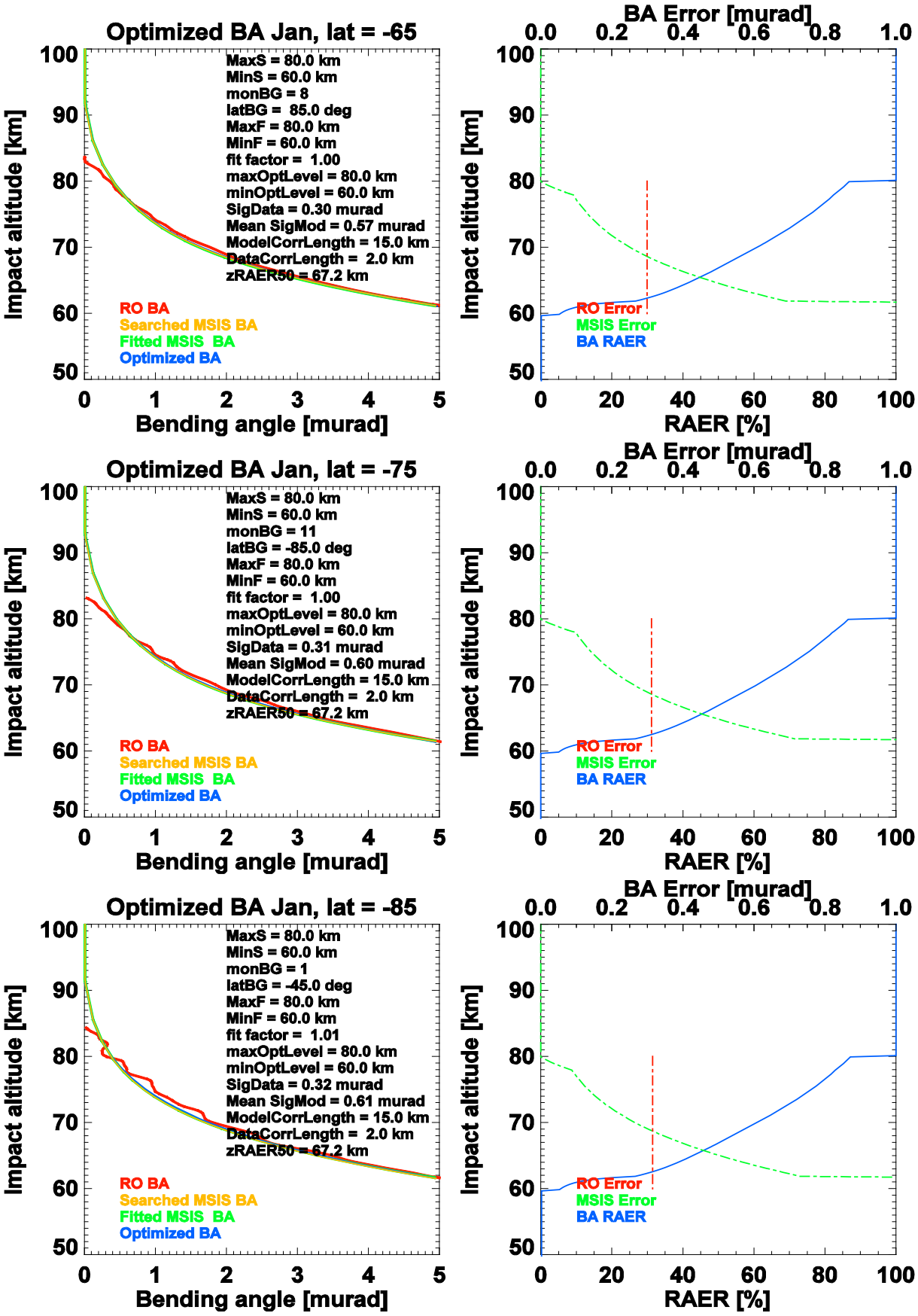

Fig. A1. Statistical optimization of RO bending angles and MSIS background for January within 10° latitude bands from North to South.

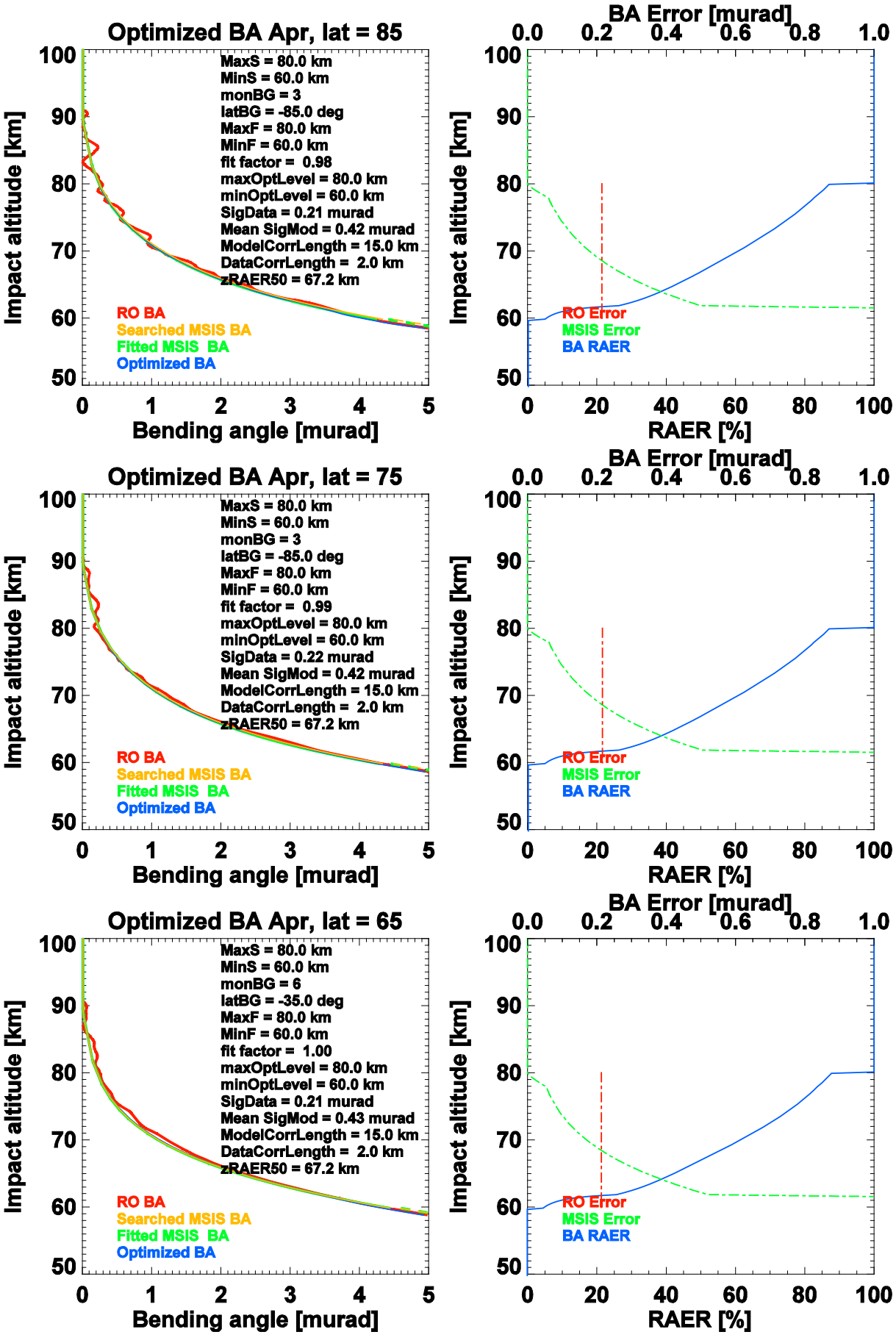
Optimized BA Apr, lat = 85
MaxS = 80.0 km
MinS = 60.0 km
monBG = 3
latBG = -85.0 deg
MaxF = 80.0 km
MinF = 60.0 km
fit factor = 0.98
maxOptLevel = 80.0 km
minOptLevel = 60.0 km
SigData = 0.21 murad
Mean SigMod = 0.42 murad
ModelCorrLength = 15.0 km
DataCorrLength = 2.0 km
zRAER50 = 67.2 km
RO BA
Searched MSIS BA
Fitted MSIS BA
Optimized BA
Impact altitude [km]
Bending angle [murad]
BA Error [murad]
RO Error
MSIS Error
BA RAER
RAER [%]
Optimized BA Apr, lat = 75
MaxS = 80.0 km
MinS = 60.0 km
monBG = 3
latBG = -85.0 deg
MaxF = 80.0 km
MinF = 60.0 km
fit factor = 0.99
maxOptLevel = 80.0 km
minOptLevel = 60.0 km
SigData = 0.22 murad
Mean SigMod = 0.42 murad
ModelCorrLength = 15.0 km
DataCorrLength = 2.0 km
zRAER50 = 67.2 km
Optimized BA Apr, lat = 65
MaxS = 80.0 km
MinS = 60.0 km
monBG = 6
latBG = -35.0 deg
MaxF = 80.0 km
MinF = 60.0 km
fit factor = 1.00
maxOptLevel = 80.0 km
minOptLevel = 60.0 km
SigData = 0.21 murad
Mean SigMod = 0.43 murad
ModelCorrLength = 15.0 km
DataCorrLength = 2.0 km
zRAER50 = 67.2 km

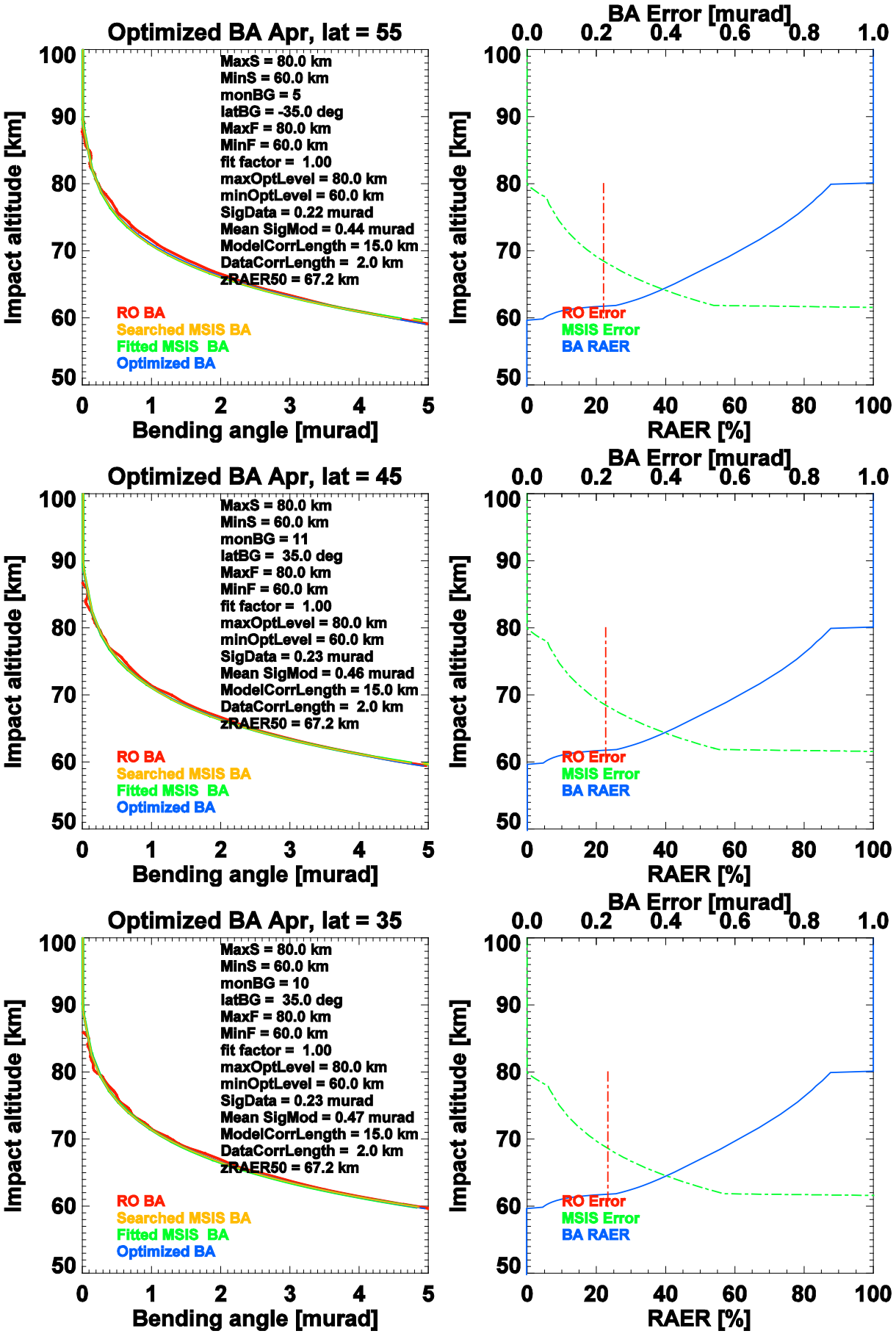
Optimized BA Apr, lat = 55
MaxS = 80.0 km
MinS = 60.0 km
monBG = 5
latBG = -35.0 deg
MaxF = 80.0 km
MinF = 60.0 km
fit factor = 1.00
maxOptLevel = 80.0 km
minOptLevel = 60.0 km
SigData = 0.22 murad
Mean SigMod = 0.44 murad
ModelCorrLength = 15.0 km
DataCorrLength = 2.0 km
zRAER50 = 67.2 km
RO BA
Searched MSIS BA
Fitted MSIS BA
Optimized BA
Impact altitude [km]
Bending angle [murad]
BA Error [murad]
RO Error
MSIS Error
BA RAER
RAER [%]
Optimized BA Apr, lat = 45
MaxS = 80.0 km
MinS = 60.0 km
monBG = 11
latBG = 35.0 deg
MaxF = 80.0 km
MinF = 60.0 km
fit factor = 1.00
maxOptLevel = 80.0 km
minOptLevel = 60.0 km
SigData = 0.23 murad
Mean SigMod = 0.46 murad
ModelCorrLength = 15.0 km
DataCorrLength = 2.0 km
zRAER50 = 67.2 km
Optimized BA Apr, lat = 35
MaxS = 80.0 km
MinS = 60.0 km
monBG = 10
latBG = 35.0 deg
MaxF = 80.0 km
MinF = 60.0 km
fit factor = 1.00
maxOptLevel = 80.0 km
minOptLevel = 60.0 km
SigData = 0.23 murad
Mean SigMod = 0.47 murad
ModelCorrLength = 15.0 km
DataCorrLength = 2.0 km
zRAER50 = 67.2 km

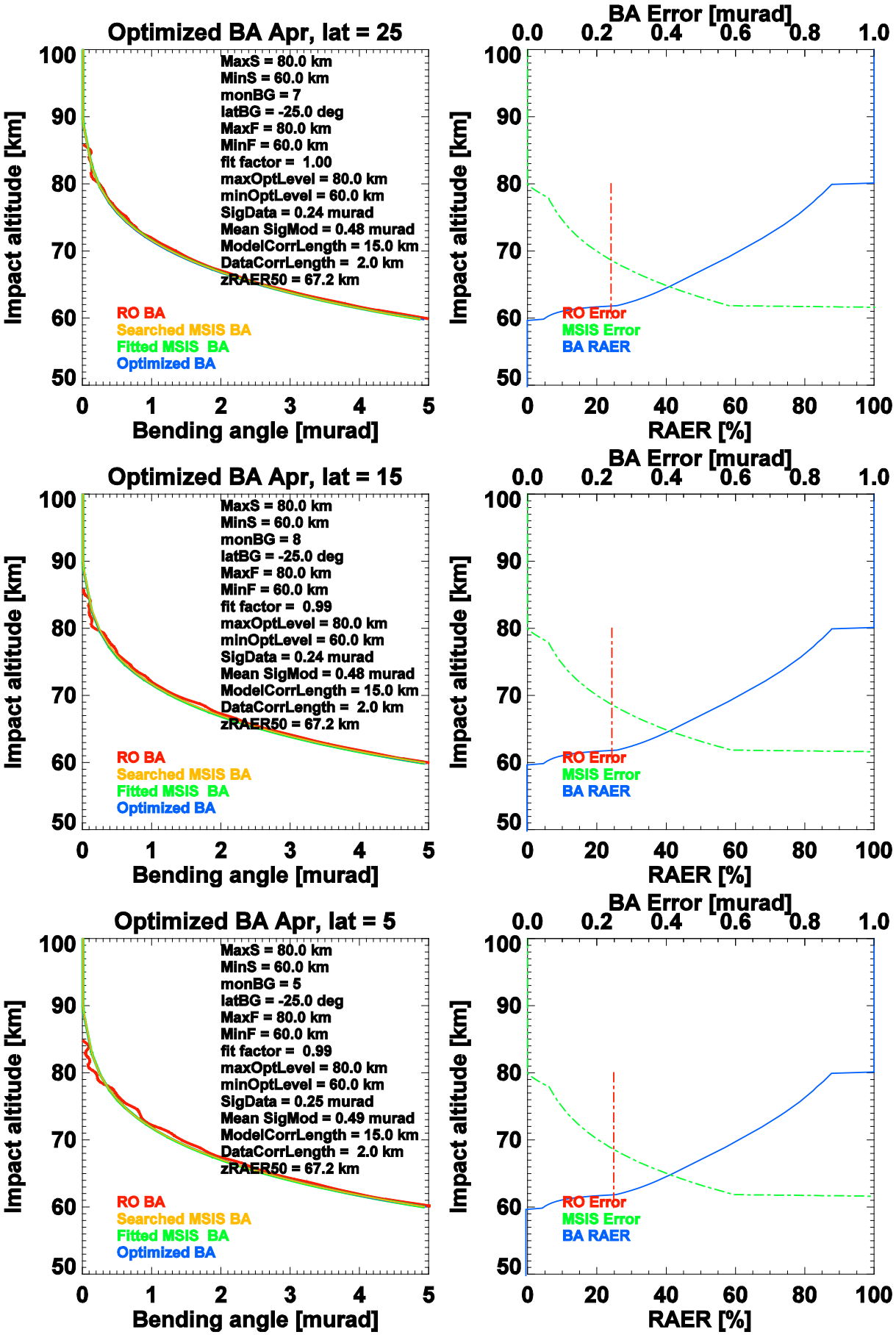
Optimized BA Apr, lat = 25
MaxS = 80.0 km
MinS = 60.0 km
monBG = 7
latBG = -25.0 deg
MaxF = 80.0 km
MinF = 60.0 km
fit factor = 1.00
maxOptLevel = 80.0 km
minOptLevel = 60.0 km
SigData = 0.24 murad
Mean SigMod = 0.48 murad
ModelCorrLength = 15.0 km
DataCorrLength = 2.0 km
zRAER50 = 67.2 km
RO BA
Searched MSIS BA
Fitted MSIS BA
Optimized BA
Impact altitude [km]
Bending angle [murad]
BA Error [murad]
RO Error
MSIS Error
BA RAER
RAER [%]
Optimized BA Apr, lat = 15
MaxS = 80.0 km
MinS = 60.0 km
monBG = 8
latBG = -25.0 deg
MaxF = 80.0 km
MinF = 60.0 km
fit factor = 0.99
maxOptLevel = 80.0 km
minOptLevel = 60.0 km
SigData = 0.24 murad
Mean SigMod = 0.48 murad
ModelCorrLength = 15.0 km
DataCorrLength = 2.0 km
zRAER50 = 67.2 km
Optimized BA Apr, lat = 5
MaxS = 80.0 km
MinS = 60.0 km
monBG = 5
latBG = -25.0 deg
MaxF = 80.0 km
MinF = 60.0 km
fit factor = 0.99
maxOptLevel = 80.0 km
minOptLevel = 60.0 km
SigData = 0.25 murad
Mean SigMod = 0.49 murad
ModelCorrLength = 15.0 km
DataCorrLength = 2.0 km
zRAER50 = 67.2 km

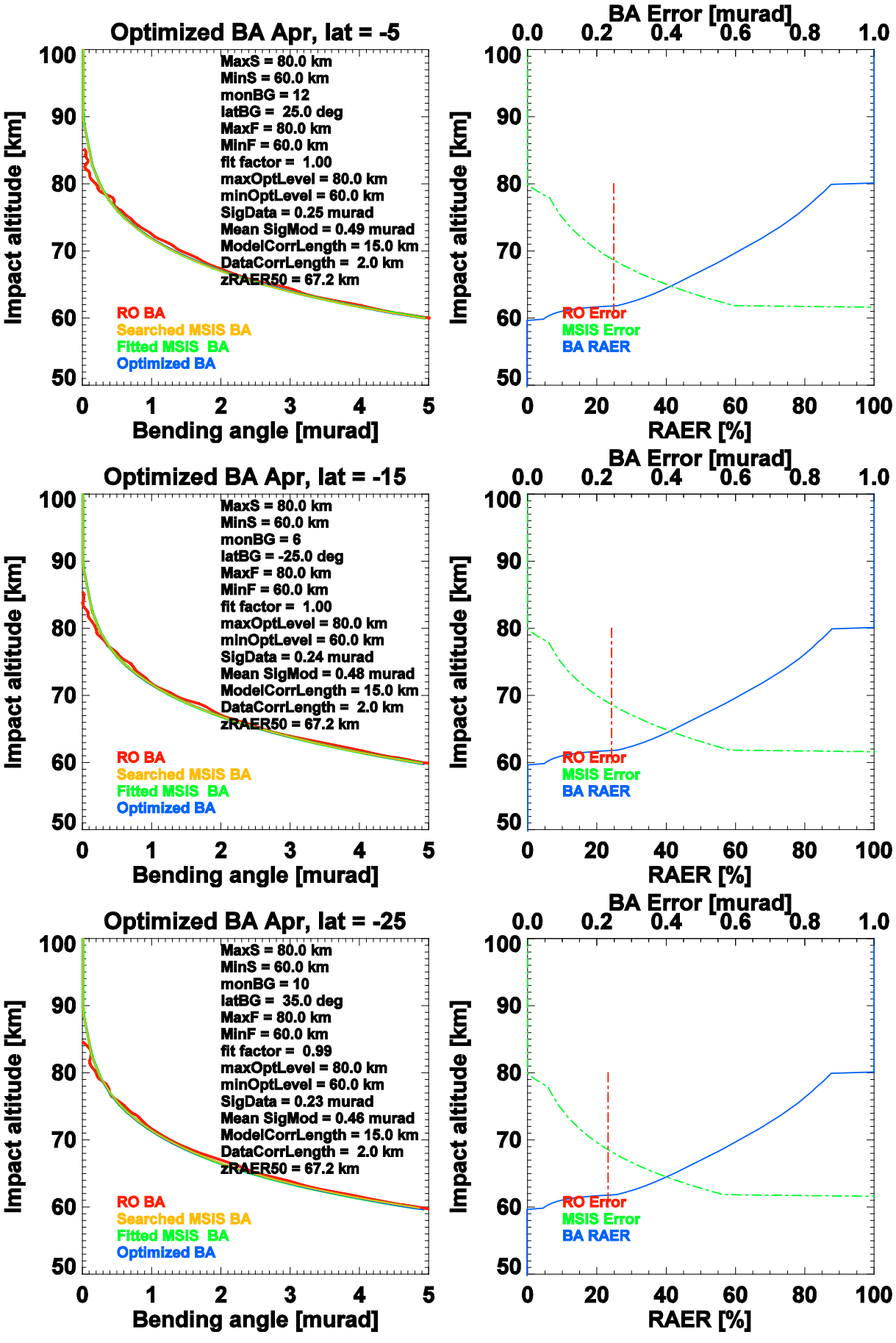
Optimized BA Apr, lat = -5
MaxS = 80.0 km
MinS = 60.0 km
monBG = 12
latBG = 25.0 deg
MaxF = 80.0 km
MinF = 60.0 km
fit factor = 1.00
maxOptLevel = 80.0 km
minOptLevel = 60.0 km
SigData = 0.25 murad
Mean SigMod = 0.49 murad
ModelCorrLength = 15.0 km
DataCorrLength = 2.0 km
zRAER50 = 67.2 km
RO BA
Searched MSIS BA
Fitted MSIS BA
Optimized BA
Impact altitude [km]
Bending angle [murad]
BA Error [murad]
RO Error
MSIS Error
BA RAER
RAER [%]
Optimized BA Apr, lat = -15
MaxS = 80.0 km
MinS = 60.0 km
monBG = 6
latBG = -25.0 deg
MaxF = 80.0 km
MinF = 60.0 km
fit factor = 1.00
maxOptLevel = 80.0 km
minOptLevel = 60.0 km
SigData = 0.24 murad
Mean SigMod = 0.48 murad
ModelCorrLength = 15.0 km
DataCorrLength = 2.0 km
zRAER50 = 67.2 km
Optimized BA Apr, lat = -25
MaxS = 80.0 km
MinS = 60.0 km
monBG = 10
latBG = 35.0 deg
MaxF = 80.0 km
MinF = 60.0 km
fit factor = 0.99
maxOptLevel = 80.0 km
minOptLevel = 60.0 km
SigData = 0.23 murad
Mean SigMod = 0.46 murad
ModelCorrLength = 15.0 km
DataCorrLength = 2.0 km
zRAER50 = 67.2 km

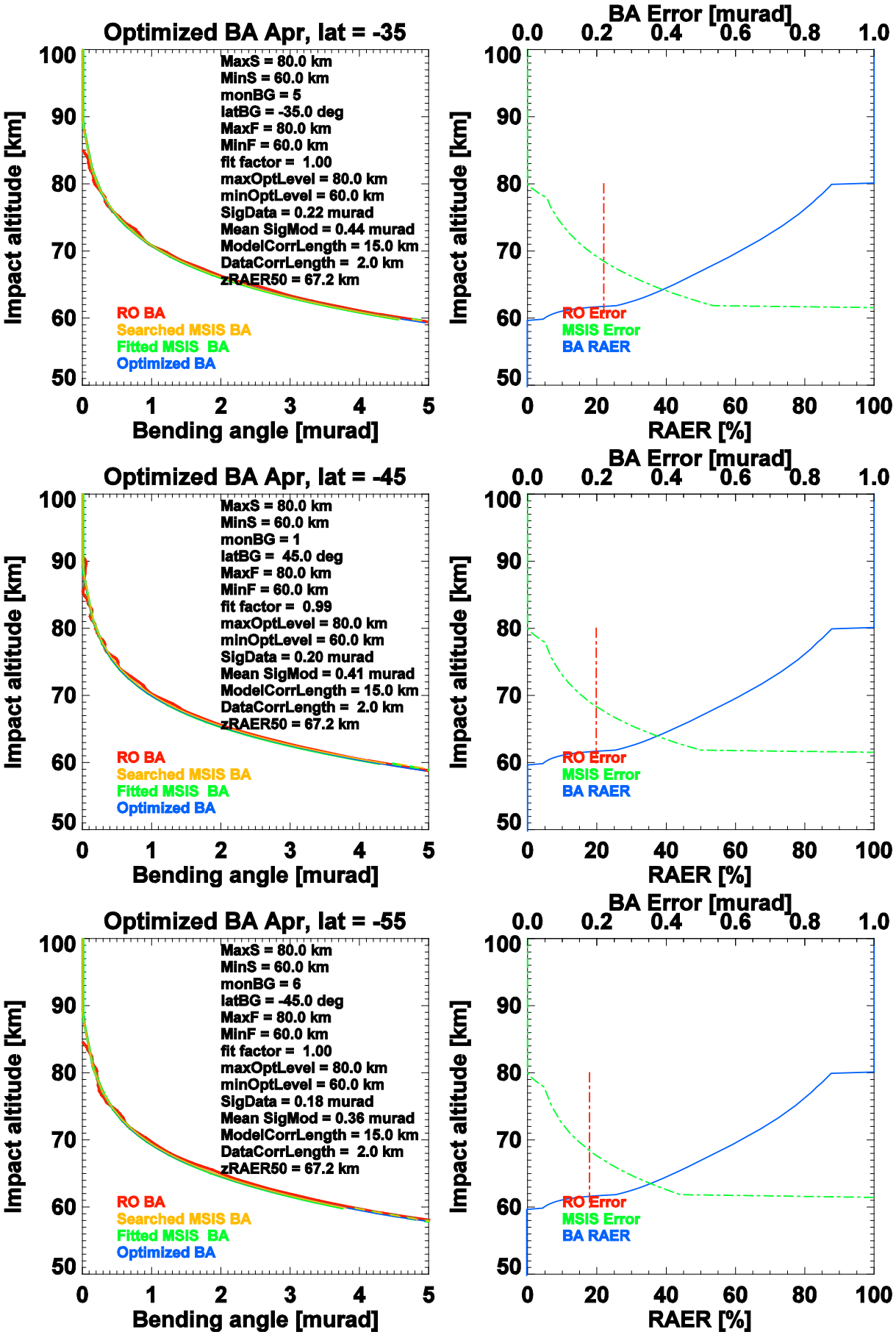
Optimized BA Apr, lat = -35
MaxS = 80.0 km
MinS = 60.0 km
monBG = 5
latBG = -35.0 deg
MaxF = 80.0 km
MinF = 60.0 km
fit factor = 1.00
maxOptLevel = 80.0 km
minOptLevel = 60.0 km
SigData = 0.22 murad
Mean SigMod = 0.44 murad
ModelCorrLength = 15.0 km
DataCorrLength = 2.0 km
zRAER50 = 67.2 km
RO BA
Searched MSIS BA
Fitted MSIS BA
Optimized BA
Impact altitude [km]
Bending angle [murad]
BA Error [murad]
RO Error
MSIS Error
BA RAER
RAER [%]
Optimized BA Apr, lat = -45
MaxS = 80.0 km
MinS = 60.0 km
monBG = 1
latBG = 45.0 deg
MaxF = 80.0 km
MinF = 60.0 km
fit factor = 0.99
maxOptLevel = 80.0 km
minOptLevel = 60.0 km
SigData = 0.20 murad
Mean SigMod = 0.41 murad
ModelCorrLength = 15.0 km
DataCorrLength = 2.0 km
zRAER50 = 67.2 km
Optimized BA Apr, lat = -55
MaxS = 80.0 km
MinS = 60.0 km
monBG = 6
latBG = -45.0 deg
MaxF = 80.0 km
MinF = 60.0 km
fit factor = 1.00
maxOptLevel = 80.0 km
minOptLevel = 60.0 km
SigData = 0.18 murad
Mean SigMod = 0.36 murad
ModelCorrLength = 15.0 km
DataCorrLength = 2.0 km
zRAER50 = 67.2 km

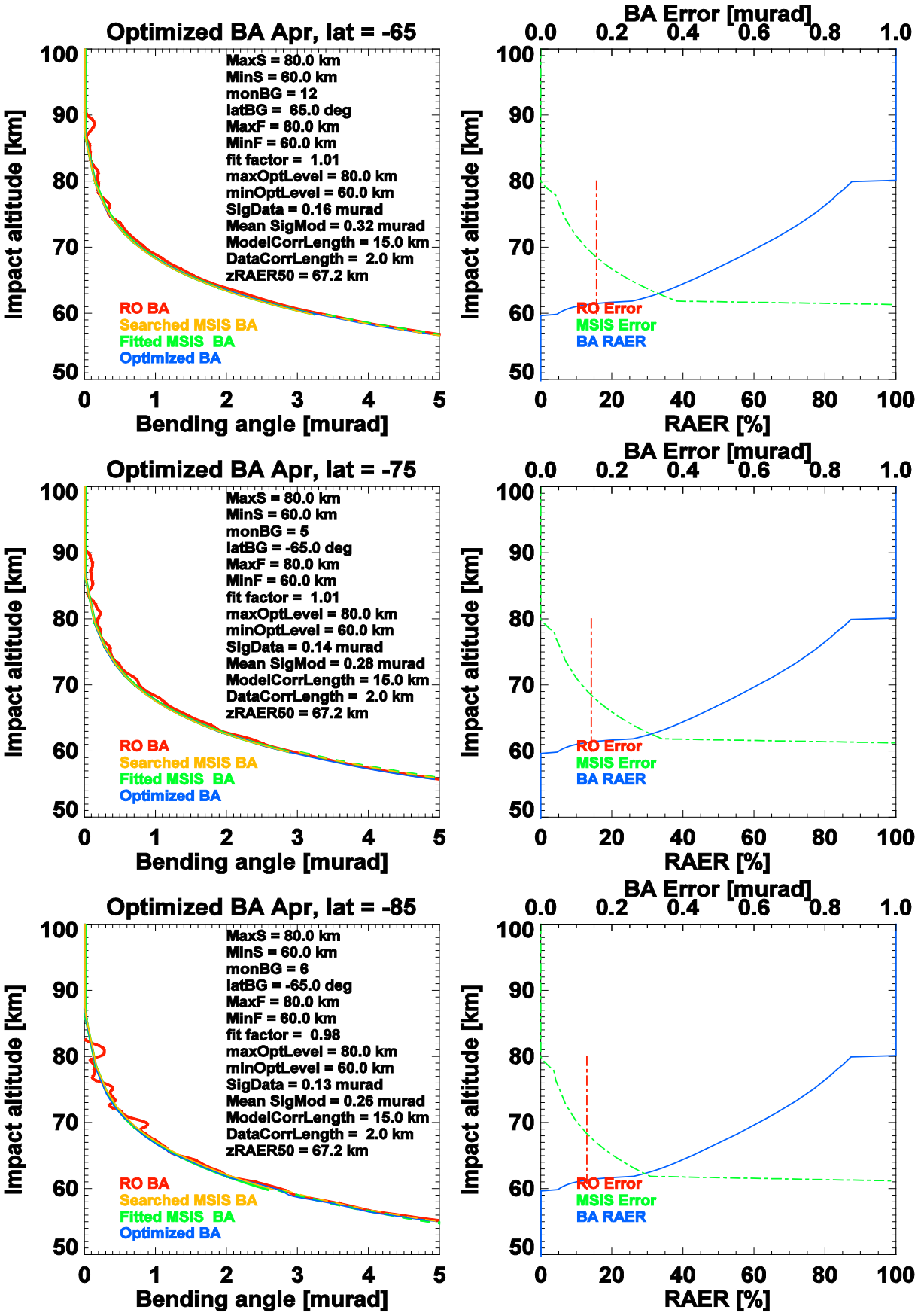

Fig. A2. Statistical optimization of RO bending angles and MSIS background for April within 10° latitude bands from North to South.

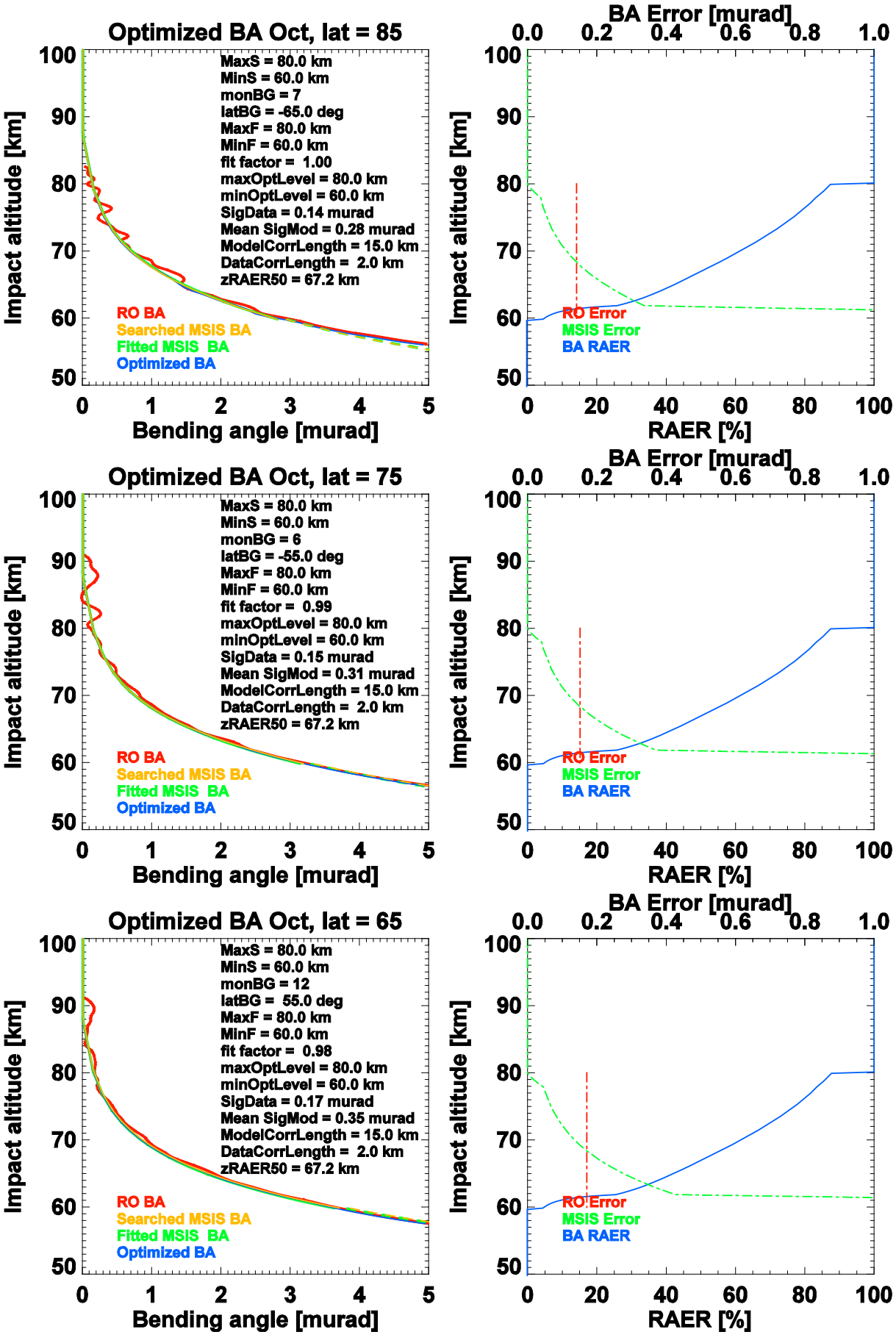
Optimized BA Oct, lat = 85
MaxS = 80.0 km
MinS = 60.0 km
monBG = 7
latBG = -65.0 deg
MaxF = 80.0 km
MinF = 60.0 km
fit factor = 1.00
maxOptLevel = 80.0 km
minOptLevel = 60.0 km
SigData = 0.14 murad
Mean SigMod = 0.28 murad
ModelCorrLength = 15.0 km
DataCorrLength = 2.0 km
zRAER50 = 67.2 km
RO BA
Searched MSIS BA
Fitted MSIS BA
Optimized BA
Impact altitude [km]
Bending angle [murad]
BA Error [murad]
RO Error
MSIS Error
BA RAER
RAER [%]
Optimized BA Oct, lat = 75
MaxS = 80.0 km
MinS = 60.0 km
monBG = 6
latBG = -55.0 deg
MaxF = 80.0 km
MinF = 60.0 km
fit factor = 0.99
maxOptLevel = 80.0 km
minOptLevel = 60.0 km
SigData = 0.15 murad
Mean SigMod = 0.31 murad
ModelCorrLength = 15.0 km
DataCorrLength = 2.0 km
zRAER50 = 67.2 km
Optimized BA Oct, lat = 65
MaxS = 80.0 km
MinS = 60.0 km
monBG = 12
latBG = 55.0 deg
MaxF = 80.0 km
MinF = 60.0 km
fit factor = 0.98
maxOptLevel = 80.0 km
minOptLevel = 60.0 km
SigData = 0.17 murad
Mean SigMod = 0.35 murad
ModelCorrLength = 15.0 km
DataCorrLength = 2.0 km
zRAER50 = 67.2 km

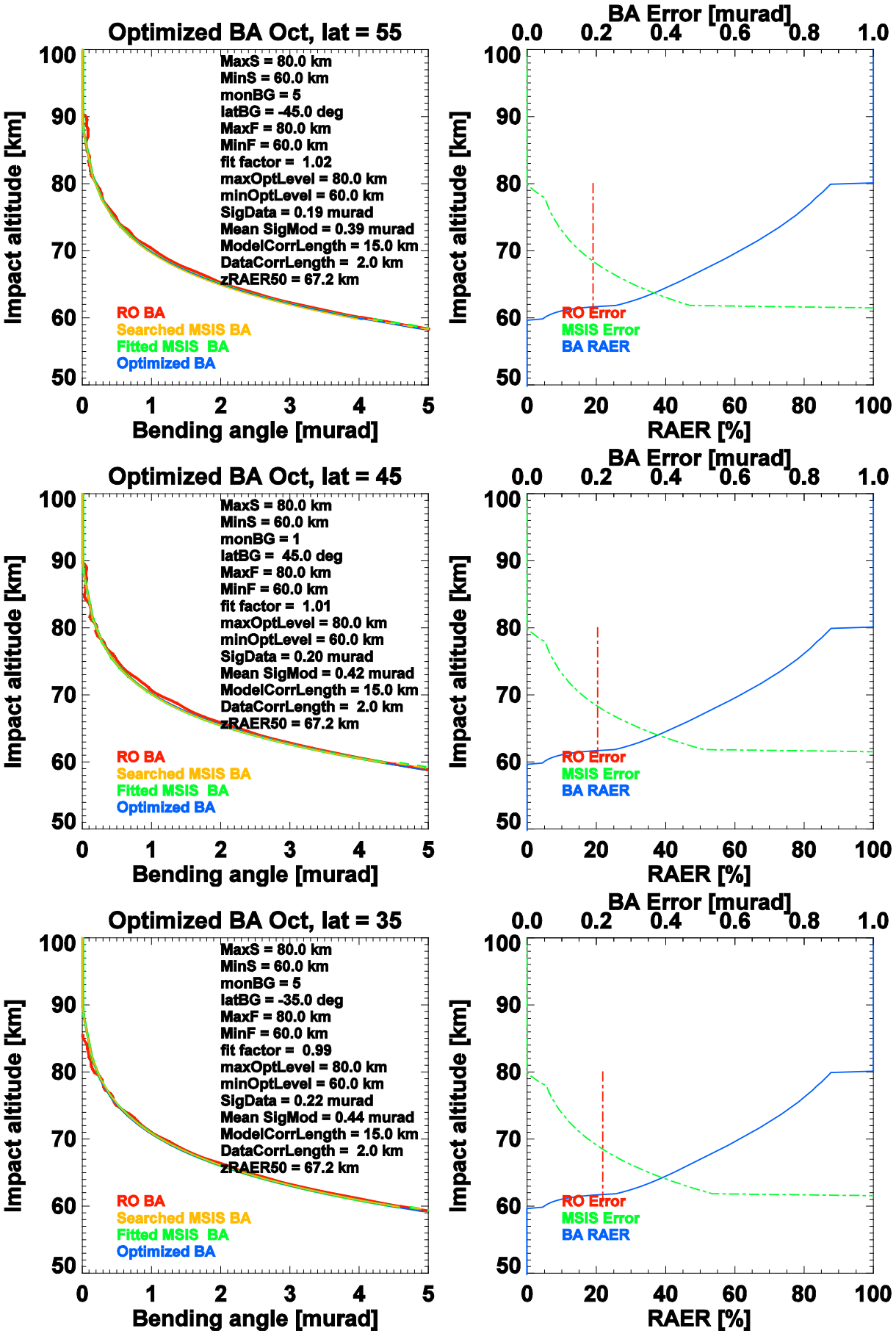
Optimized BA Oct, lat = 55
MaxS = 80.0 km
MinS = 60.0 km
monBG = 5
latBG = -45.0 deg
MaxF = 80.0 km
MinF = 60.0 km
fit factor = 1.02
maxOptLevel = 80.0 km
minOptLevel = 60.0 km
SigData = 0.19 murad
Mean SigMod = 0.39 murad
ModelCorrLength = 15.0 km
DataCorrLength = 2.0 km
zRAER50 = 67.2 km
RO BA
Searched MSIS BA
Fitted MSIS BA
Optimized BA
Impact altitude [km]
Bending angle [murad]
BA Error [murad]
RO Error
MSIS Error
BA RAER
RAER [%]
Optimized BA Oct, lat = 45
MaxS = 80.0 km
MinS = 60.0 km
monBG = 1
latBG = 45.0 deg
MaxF = 80.0 km
MinF = 60.0 km
fit factor = 1.01
maxOptLevel = 80.0 km
minOptLevel = 60.0 km
SigData = 0.20 murad
Mean SigMod = 0.42 murad
ModelCorrLength = 15.0 km
DataCorrLength = 2.0 km
zRAER50 = 67.2 km
Optimized BA Oct, lat = 35
MaxS = 80.0 km
MinS = 60.0 km
monBG = 5
latBG = -35.0 deg
MaxF = 80.0 km
MinF = 60.0 km
fit factor = 0.99
maxOptLevel = 80.0 km
minOptLevel = 60.0 km
SigData = 0.22 murad
Mean SigMod = 0.44 murad
ModelCorrLength = 15.0 km
DataCorrLength = 2.0 km
zRAER50 = 67.2 km

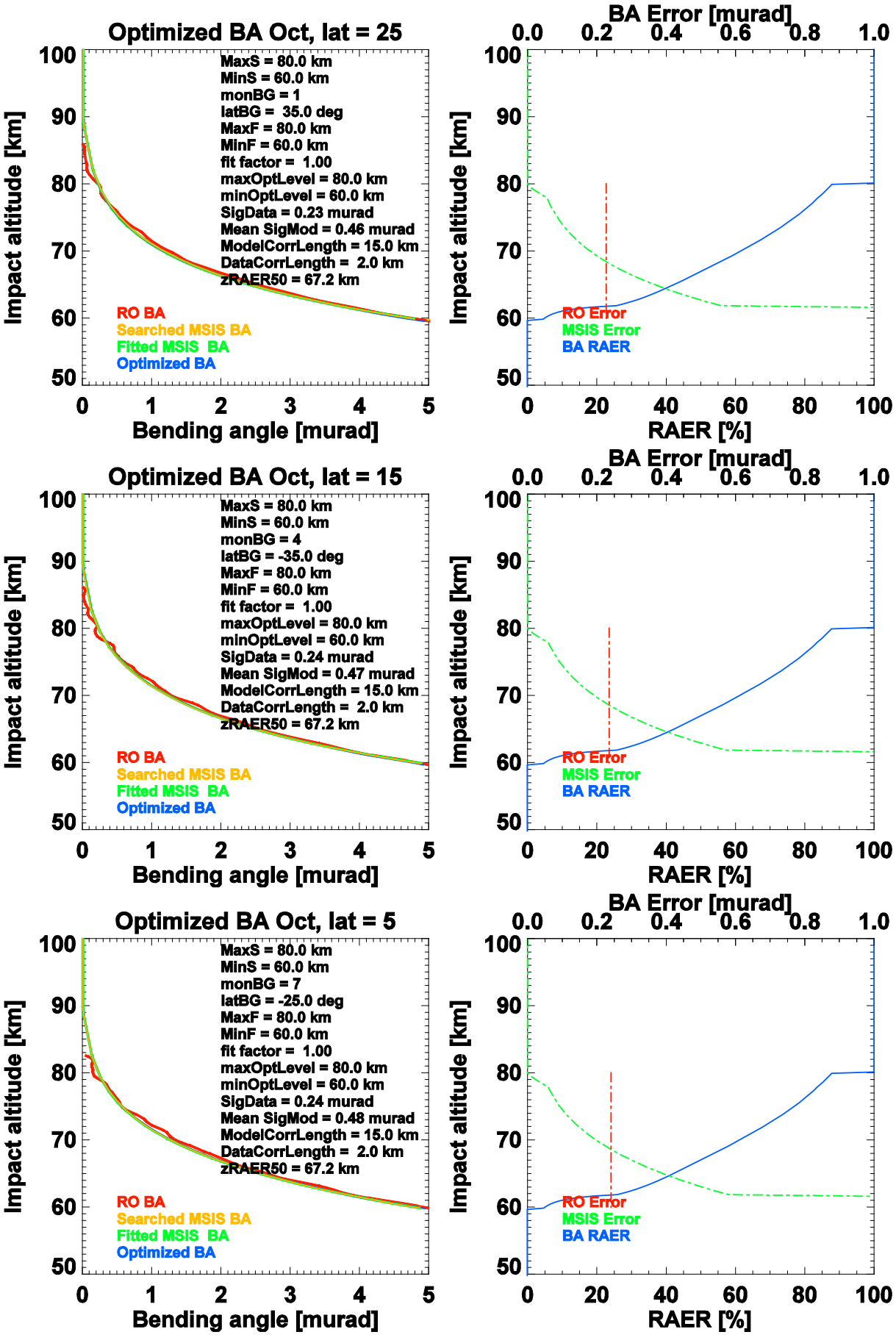
Optimized BA Oct, lat = 25
MaxS = 80.0 km
MinS = 60.0 km
monBG = 1
latBG = 35.0 deg
MaxF = 80.0 km
MinF = 60.0 km
fit factor = 1.00
maxOptLevel = 80.0 km
minOptLevel = 60.0 km
SigData = 0.23 murad
Mean SigMod = 0.46 murad
ModelCorrLength = 15.0 km
DataCorrLength = 2.0 km
zRAER50 = 67.2 km
RO BA
Searched MSIS BA
Fitted MSIS BA
Optimized BA
Impact altitude [km]
Bending angle [murad]
BA Error [murad]
RO Error
MSIS Error
BA RAER
RAER [%]
Optimized BA Oct, lat = 15
MaxS = 80.0 km
MinS = 60.0 km
monBG = 4
latBG = -35.0 deg
MaxF = 80.0 km
MinF = 60.0 km
fit factor = 1.00
maxOptLevel = 80.0 km
minOptLevel = 60.0 km
SigData = 0.24 murad
Mean SigMod = 0.47 murad
ModelCorrLength = 15.0 km
DataCorrLength = 2.0 km
zRAER50 = 67.2 km
Optimized BA Oct, lat = 5
MaxS = 80.0 km
MinS = 60.0 km
monBG = 7
latBG = -25.0 deg
MaxF = 80.0 km
MinF = 60.0 km
fit factor = 1.00
maxOptLevel = 80.0 km
minOptLevel = 60.0 km
SigData = 0.24 murad
Mean SigMod = 0.48 murad
ModelCorrLength = 15.0 km
DataCorrLength = 2.0 km
zRAER50 = 67.2 km

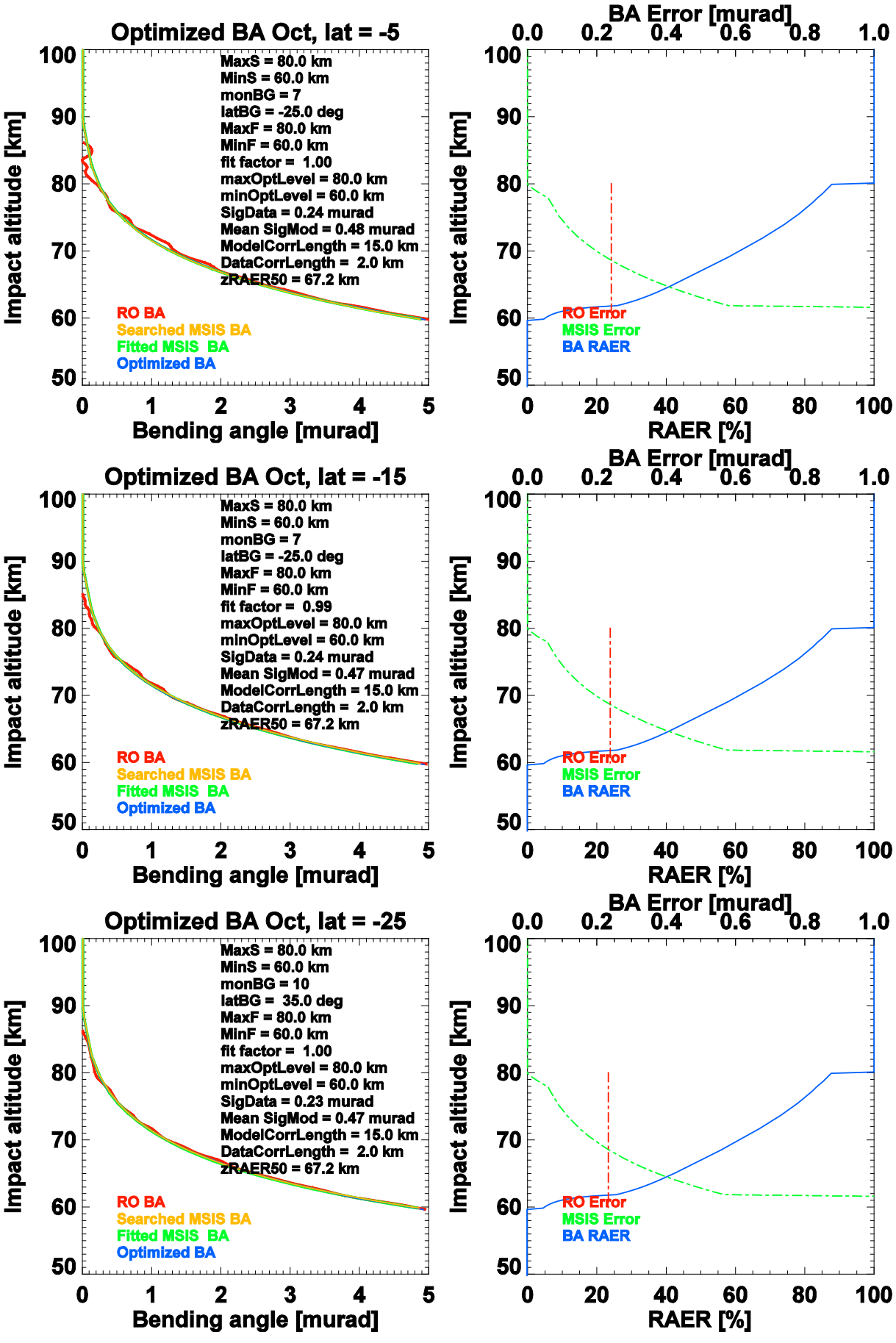
Optimized BA Oct, lat = -5
MaxS = 80.0 km
MinS = 60.0 km
monBG = 7
latBG = -25.0 deg
MaxF = 80.0 km
MinF = 60.0 km
fit factor = 1.00
maxOptLevel = 80.0 km
minOptLevel = 60.0 km
SigData = 0.24 murad
Mean SigMod = 0.48 murad
ModelCorrLength = 15.0 km
DataCorrLength = 2.0 km
zRAER50 = 67.2 km
RO BA
Searched MSIS BA
Fitted MSIS BA
Optimized BA
Impact altitude [km]
Bending angle [murad]
BA Error [murad]
RO Error
MSIS Error
BA RAER
RAER [%]
Optimized BA Oct, lat = -15
MaxS = 80.0 km
MinS = 60.0 km
monBG = 7
latBG = -25.0 deg
MaxF = 80.0 km
MinF = 60.0 km
fit factor = 0.99
maxOptLevel = 80.0 km
minOptLevel = 60.0 km
SigData = 0.24 murad
Mean SigMod = 0.47 murad
ModelCorrLength = 15.0 km
DataCorrLength = 2.0 km
zRAER50 = 67.2 km
Optimized BA Oct, lat = -25
MaxS = 80.0 km
MinS = 60.0 km
monBG = 10
latBG = 35.0 deg
MaxF = 80.0 km
MinF = 60.0 km
fit factor = 1.00
maxOptLevel = 80.0 km
minOptLevel = 60.0 km
SigData = 0.23 murad
Mean SigMod = 0.47 murad
ModelCorrLength = 15.0 km
DataCorrLength = 2.0 km
zRAER50 = 67.2 km

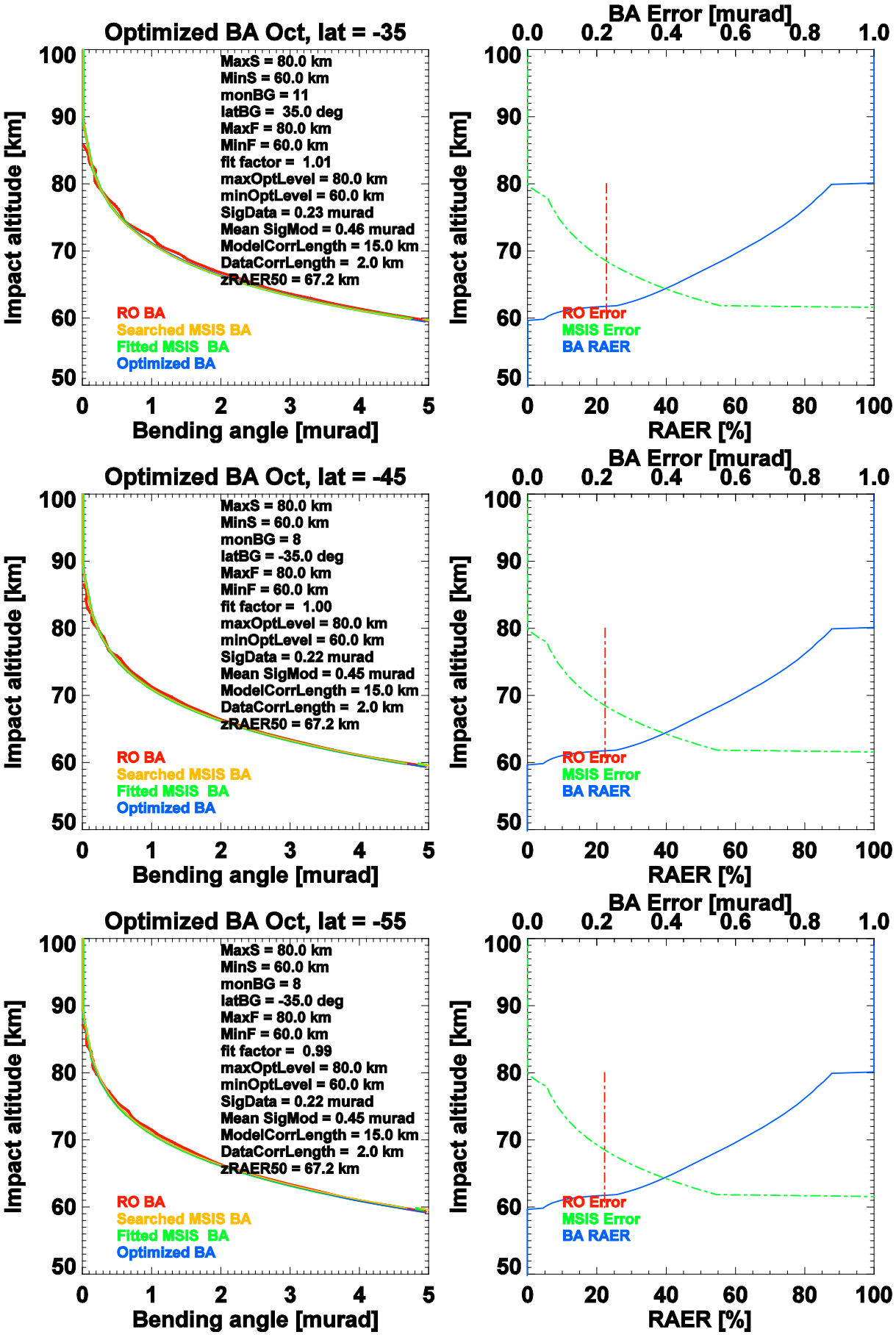
Optimized BA Oct, lat = -35
MaxS = 80.0 km
MinS = 60.0 km
monBG = 11
latBG = 35.0 deg
MaxF = 80.0 km
MinF = 60.0 km
fit factor = 1.01
maxOptLevel = 80.0 km
minOptLevel = 60.0 km
SigData = 0.23 murad
Mean SigMod = 0.46 murad
ModelCorrLength = 15.0 km
DataCorrLength = 2.0 km
zRAER50 = 67.2 km
RO BA
Searched MSIS BA
Fitted MSIS BA
Optimized BA
Impact altitude [km]
Bending angle [murad]
BA Error [murad]
RO Error
MSIS Error
BA RAER
RAER [%]
Optimized BA Oct, lat = -45
MaxS = 80.0 km
MinS = 60.0 km
monBG = 8
latBG = -35.0 deg
MaxF = 80.0 km
MinF = 60.0 km
fit factor = 1.00
maxOptLevel = 80.0 km
minOptLevel = 60.0 km
SigData = 0.22 murad
Mean SigMod = 0.45 murad
ModelCorrLength = 15.0 km
DataCorrLength = 2.0 km
zRAER50 = 67.2 km
Optimized BA Oct, lat = -55
MaxS = 80.0 km
MinS = 60.0 km
monBG = 8
latBG = -35.0 deg
MaxF = 80.0 km
MinF = 60.0 km
fit factor = 0.99
maxOptLevel = 80.0 km
minOptLevel = 60.0 km
SigData = 0.22 murad
Mean SigMod = 0.45 murad
ModelCorrLength = 15.0 km
DataCorrLength = 2.0 km
zRAER50 = 67.2 km

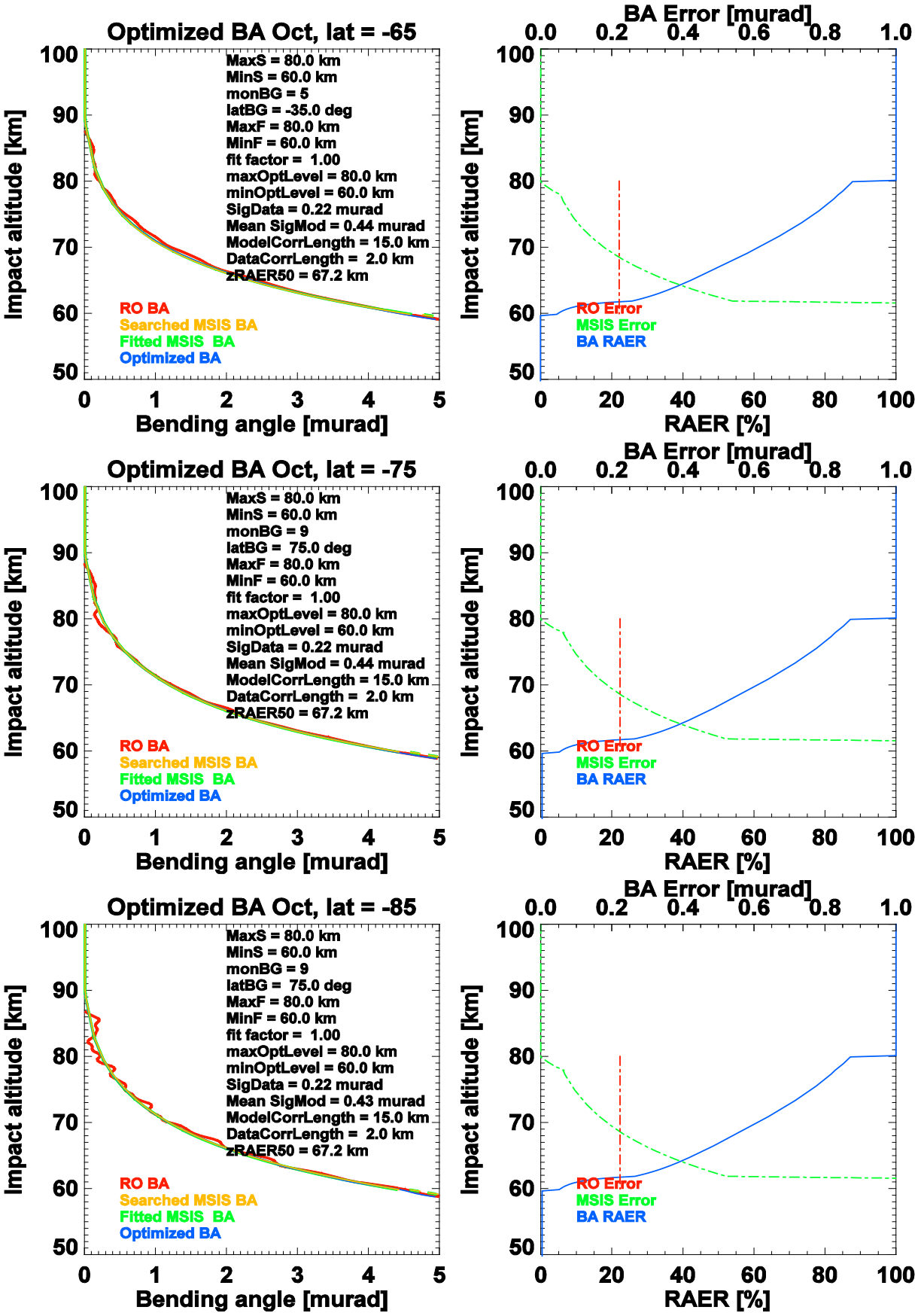

Fig. A3. Statistical optimization of RO bending angles and MSIS background for October within 10° latitude bands from North to South.